

INCREASING THE EFFICIENCY OF GEOTHERMAL POWER PLANTS USING OPTIMUM PRESSURES  
FOR TURBOCOMPRESSORS AND STEAM JET EJECTORS IN GAS EXTRACTION SYSTEMS

By

Karsten Franz Harns

A THESIS

Submitted to  
Michigan State University  
in partial fulfillment of the requirements  
for the degree of

Mechanical Engineering – Master of Science

2014

## ABSTRACT

### INCREASING THE EFFICIENCY OF GEOTHERMAL POWER PLANTS USING OPTIMUM PRESSURES FOR TURBOCOMPRESSORS AND STEAM JET EJECTORS IN GAS EXTRACTION SYSTEMS

By

Karsten Franz Harns

Geothermal power plants generate electricity by extracting energy from the earth's interior. The radioactive decay of the earth's core causes heat to conduct towards the surface. When water flows into the fissures of this hot rock a naturally occurring geothermal well is formed. Geothermal power plants use the steam in these wells to drive a turbine and thus generate electricity.

The steam in the earth however, is always accompanied by a small fraction of non-condensable gases that build up in the power plant's condenser unless actively removed by some gas extraction system. Because these gases contribute significantly to the total backpressure on the turbine, it is in the interest of power generation to remove them from the condenser. The industry standard for removing these non-condensable gases has been steam jet ejectors or a hybrid system of steam jet ejectors and liquid ring vacuum pumps. This thesis focuses on finding the optimum operating pressures for a hybrid steam jet ejector system and a hybrid turbocompressor system. It was found that plants with steam jet ejectors and liquid ring vacuum pumps provide maximum power output when the liquid ring vacuum pump is operated at its maximum pressure ratio. However, plants with a turbocompressor and liquid ring vacuum pump were found to provide maximum power output when the turbocompressor was operated at its maximum pressure ratio.

Copyright by  
KARSTEN FRANZ HARNIS  
2014

## ACKNOWLEDGEMENTS

I would like to thank my thesis adviser, Dr. Norbert Mueller for the many hours of guidance and instruction he has provided me both inside and outside of the classroom. His expertise in turbomachinery and engineering thermodynamics has been invaluable to my education at Michigan State University. I would also like to thank my committee members, Drs. Abraham Engeda and Dahsin Liu for their time and help.

## TABLE OF CONTENTS

LIST OF TABLES .....	vi
LIST OF FIGURES .....	vii
KEY TO ABBREVIATIONS .....	ix
CHAPTER 1.0 .....	1
1.1 Introduction to Geothermal Power Generation .....	1
1.2 Types of Geothermal Power Plants .....	2
1.3 The Problem of Non-Condensable Gases and Current Gas Extraction Systems .....	3
CHAPTER 2.0 .....	12
2.1 Thermodynamic Model Assumptions for Flash Steam Geothermal Power Plants .....	12
2.2 Methods Used to Compare the Performance of Geothermal Gas Extraction Systems ...	15
CHAPTER 3.0 .....	28
3.1 Case Study of a Typical Flash Steam Plant .....	28
CHAPTER 4.0 .....	44
4.1 Conclusions .....	44
4.2 Potential Future Work .....	45
APPENDIX .....	46
REFERENCES .....	53

LIST OF TABLES

Table 1: Coefficients of the Cp Polynomial..... 17

## LIST OF FIGURES

Figure 1: Fluid Pressure and Velocity Changes Through the SJE .....	7
Figure 2: A Prototype Impeller of the Compressor with Integrated Magnets in the Shroud (left), and the Prototype 10 stage, Counter-Rotating, NCG Compressor (right).....	11
Figure 3: General Layout of a Single-Flash Power Plant .....	13
Figure 4: The Flash Plant Cycle on a Temperature-Entropy Diagram.....	15
Figure 5: Temperature Entrainment Ratio Curves.....	20
Figure 6: Molecular Weight Entrainment Ratio Curve .....	21
Figure 7: Relation Between Expansion Ratio, Compression Ratio, and Air to Steam Ratio .....	23
Figure 8: Typical Operational Pressures in a Geothermal GES .....	30
Figure 9: Optimum Condenser Pressure Diagram for Case 1 .....	31
Figure 10: Optimum Condenser Pressure Diagram for Case 2 .....	32
Figure 11: Net Power Output Diagram for Case 1 .....	33
Figure 12: Net Power Output Diagram for Case 2 .....	34
Figure 13: Power Consumption for Case 1 .....	35
Figure 14: Power Consumption for Case 2 .....	36
Figure 15: Difference in Net Power Output for Case 1.....	37
Figure 16: Difference in Net Power Output for Case 2.....	37
Figure 17: Change in Specific Heat for Case 1 .....	38
Figure 18: Change in Specific Heat for Case 2 .....	39
Figure 19: Mass Flow Rates for Case 1 .....	40
Figure 20: Mass Flow Rates for Case 2 .....	40

Figure 21: Outlet Temperatures for Case 1 .....	41
Figure 22: Outlet Temperatures for Case 2 .....	42
Figure 23: Mixture Molecular Weight for Case 1 .....	43
Figure 24: Mixture Molecular Weight for Case 2 .....	43
Figure 25: Optimum Pressure at 12° Celsius for Case 1 .....	47
Figure 26: Optimum Pressure at 12° Celsius for Case 2 .....	47
Figure 27: Optimum Pressure at 22.22° Celsius for Case 1 .....	48
Figure 28: Optimum Pressure at 22.22° Celsius for Case 2 .....	48
Figure 29: Optimum Pressure at 28.33° Celsius for Case 1 .....	49
Figure 30: Optimum Pressure at 28.33° Celsius for Case 2 .....	49
Figure 31: Optimum Pressure at 35° Celsius for Case 1 .....	50
Figure 32: Optimum Pressure at 35° Celsius for Case 2 .....	50
Figure 33: Optimum Pressure at 36.1° Celsius for Case 1 .....	51
Figure 34: Optimum Pressure at 36.1° Celsius for Case 2 .....	51
Figure 35: Optimum Pressure at 42° Celsius for Case 1 .....	52
Figure 36: Optimum Pressure at 42° Celsius for Case 2 .....	52

## KEY TO ABBREVIATIONS

ASR .....	Air to Steam Ratio [kg/kg]
$c_p$ .....	Constant Pressure Specific Heat Constant [kJ/kg*K]
$c_v$ .....	Constant Volume Specific Heat Constant [kJ/kg*K]
CR .....	Compression Ratio [kPa/kPa]
DAE .....	Dry Air Equivalent Mass Flow Rate[kg/s]
$\tilde{e}$ .....	Mass Specific Shaft Work [kJ/kg]
EGS .....	Enhanced Geothermal Systems
ER .....	Expansion Ratio [kPa/kPa]
GEA.....	Geothermal Energy Association
GES .....	Gas Extraction System
$h$ .....	Mass Specific Enthalpy [kJ/kg]
$\bar{h}$ .....	Molar Specific Enthalpy [kJ/kg]
HEI .....	Heat Exchange Institute
LRVP .....	Liquid Ring Vacuum Pump
$M$ .....	Molecular Weight [kg/kmol]
$\dot{m}$ .....	Mass Flow Rate [kg/s]
$m_f$ .....	Mass Fraction [kg/kg]
MSC .....	Motive Steam Consumption[kg/s]
$n$ .....	Number of Moles [kmol]

NCG ..... Non-Condensable Gases

P ..... Power [MW]

p ..... Pressure [kPa]

R ..... Specific Gas Constant [J/kg\*K]

s ..... Mass Specific Entropy [kJ/kg]

$\bar{s}$  ..... Molar Specific Entropy [kJ/kg]

SJE ..... Steam Jet Ejector

T ..... Temperature [K]

TER ..... Temperature Entrainment Ratio [ $^{\circ}\text{C} / ^{\circ}\text{C}$ ]

WER ..... Weight Entrainment Ratio [kg/kg]

WW ..... Woven Wheel

y ..... Mole Fraction [kmol/kmol]

$\eta$  ..... Efficiency [MW/MW]

$\gamma$  ..... Specific Heat Ratio [(kJ/kg\*K) / (kJ/kg\*K)]

## CHAPTER 1.0

### 1.1 Introduction to Geothermal Power Generation

Geothermal power generation is the harnessing of energy deep in the earth's crust for the purpose of generating electricity. Etymologically, the word geothermal comes from the combination of geo, meaning earth and thermal, meaning heat. For thousands of years humans have made use of the earth's heat, particularly in volcanic areas for the purpose of cooking, heating, spa bathing and even for medicinal reasons (1). It was not until the turn of the 20<sup>th</sup> century however, that steam in the earth was used for power generation. The first geothermal power plant was built in Larderello, Italy in 1904 and Enel Power continues to produce power from the same geothermal field today (2).

Over the last hundred years geothermal energy has attracted significant interest around the globe because it is considered a reliable, renewable resource with extremely low carbon emissions. Unlike wind and solar energy, geothermal wells can provide sustainable base load power indefinitely if managed properly. Geothermal power plants are an environmentally attractive solution to the world's energy needs as they produce on average 12 times less the carbon dioxide emissions of coal-fired power plants and 6 times less than natural-gas-fired power plants (3). For this reason, energy policy makers and energy companies are seeking to advance technologies such as Enhanced Geothermal Systems (EGS) in order to create man-made geothermal wells and thereby drastically increase the worldwide viability of geothermal power generation.

## 1.2 Types of Geothermal Power Plants

Three main types of geothermal power plants exist today. Each type is designed based on the temperature and phase of the geothermal resource. Dry steam plants are built where the geothermal resource is already significantly vaporized as it comes out of the well. These were the first geothermal power plants built and they still account for the greatest geothermal generating capacity in the United States. The majority of dry steam plants in the United States are owned and operated by Calpine Corporation at The Geysers geothermal field in northern California. The total U.S. installed capacity of dry steam power plants in 2012 was 1585 megawatts, which accounts for nearly 50% of the United States' geothermal power production (3).

Flash steam plants on the other hand are built where a significant portion of the geothermal resource is still liquid. The process of vaporizing the resource distinguishes flash plants. These plants use a steam separator to suddenly decrease the fluid pressure and thereby rapidly vaporize a portion of the high-pressure water that comes from the geothermal well. Like dry steam plants, the vapor is then used to drive a turbine and generate power. The portion of the water that does not vaporize in the steam separator, known as brine, is either reinjected to the geothermal well or passes through a heat exchanger to power a binary cycle plant. The total U.S. installed capacity of flash steam power plants in 2012 was 900 megawatts. This accounts for approximately 28% of geothermal power production in the United States (3).

Binary plants are the fastest growing of all three plant types as they have permitted geothermal power generation in locations where resources were previously considered to be nonviable due to low temperatures and pressures. Binary plants make use of geothermal

resources that are considered too cool to generate power in a dry or flash steam plant. These plants use heat exchangers to transfer energy from the geothermal resource to a secondary fluid with a lower boiling point. This secondary fluid then vaporizes and can be used to drive a turbine for power generation in a closed loop cycle. Due to their low boiling points, isobutene and pentafluoropropane are frequently used as the secondary fluid. The Kalina cycle is a common binary cycle that uses an ammonia-water mixture. As of 2012, the total U.S. installed capacity of binary power plants was 702 megawatts, accounting for approximately 22% of U.S. geothermal power production (3).

The Geothermal Energy Association (GEA) reported in 2012 that 3% of renewable energy-based electricity consumption in the United States came from geothermal resources in the western states of California, Nevada and Oregon (3). Due to rock permeability and high temperatures at comparatively shallow depths in these states, these resources are referred to as the low-hanging fruit of the industry. However, the GEA estimates that only 10% of these resources have been developed yet, leaving significant room for growth. Even so, U.S. geothermal energy production is currently greater than any other nation, accounting for nearly 28% of the world's total production. Since the world's greatest undeveloped geothermal capacity is outside the United States however, the GEA states "opportunities for U.S. geothermal companies abound in the global market" (3).

### 1.3 The Problem of Non-Condensable Gases and Current Gas Extraction Systems

As the steam comes out of the geothermal wells it is always accompanied by a small fraction of Non-Condensable Gases (NCG). These gases are so named, because they do not

condense at the condensation pressure and temperature of H<sub>2</sub>O in the condenser and therefore cannot be removed by the condensate pump. Depending on the specific conditions of the geothermal field, these gases can range from less than a percent to as high as 5 percent by mass fraction of the total steam. While they can include CO<sub>2</sub>, H<sub>2</sub>S, CH<sub>4</sub>, NH<sub>3</sub>, N<sub>2</sub>, and C<sub>2</sub>H<sub>6</sub> in various concentrations depending on the specific geothermal well, CO<sub>2</sub> typically accounts for 80% of the total NCG (4). For binary plants, the presence of NCG in the geothermal resource is of negligible concern compared to dry and flash steam plants. This is because NCG in the secondary cycle fluid is extremely small and typically exists because of air leakage from the surroundings into the low-pressure system. The primary concern in dry and flash steam plants however comes from NCG entrained in the steam coming from the geothermal well. This causes adverse effects on the performance of the condenser and hence the efficiency and power output of the cycle.

The presence of NCG decreases the condenser's heat transfer efficiency as the specific heat of CO<sub>2</sub> is less than half that of H<sub>2</sub>O at the same temperature. This increases the surface area requirements of the condenser, which leads to higher capital costs. In addition to this, if the NCG is not continuously removed from the condenser, it contributes a significant backpressure to the turbine and thereby decreases the power generation of the plant. Because CO<sub>2</sub> and H<sub>2</sub>S are both water soluble, their corrosive presence can have adverse effects on the equipment. Lastly, the cooling needs of a plant typically increase with increased levels of NCG. After being pumped out of the condenser, the NCG has a higher temperature and pressure as it

enters the inter-condenser and after-condensers. Therefore higher NCG concentrations will increase the necessary auxiliary power to run the cooling towers that supply water to these smaller condensers (4).

Because the presence of NCG in the condenser significantly decreases the thermal efficiency and power output of a plant, multiple Gas Extraction Systems (GES) have been designed to remove NCG. These include:

1. Liquid Ring Vacuum Pumps (LRVP)
2. Steam Jet Ejectors (SJE)
3. Hybrid Systems of Steam Jet Ejectors and Liquid Ring Vacuum Pumps
4. Centrifugal Compressors

Each of these systems has costs and benefits thermodynamically and economically. These must be evaluated at the particular conditions of each plant in order to determine the optimum gas extraction system.

Liquid ring vacuum pumps are a kind of rotating positive displacement pump. They essentially consist of a vaned impeller on a shaft inside a cylindrical casing. As it rotates, water or some other liquid is fed into the pump and centrifugal forces from the impeller's rotation cause the liquid to form a spinning ring on the inside of the casing. The impeller shaft however, is designed to be eccentric from the center of the casing in order to create cells of changing volume. The NCG mixture is fed into these cells, compressed and expelled from the pump.

While LRVP are frequently used as a final stage in a series of SJE, their inability to operate at extremely low pressures restricts their possible application for use in early stages of compression. In most geothermal plants the condenser pressure is far below atmospheric

pressure and this would cause the ring of liquid in the pump, typically water, to evaporate as the pressure decreased below the vapor pressure of the liquid in the ring. As a result, the pump's compression capacity decreases as the ring becomes smaller and smaller. Hence, LRVP are primarily used as a final stage in a series of SJE. They have efficiencies up to 50% (5), which is nearly 3 times greater than SJE, however their capital cost is approximately 5 times greater than SJE (6).

By far the most commonly installed GES in flash and dry steam plants are steam jet ejectors. Their ubiquitous presence is due to their low capital cost, simple design, no moving parts and hence minimal maintenance requirements. They are vacuum pumps that operate on the basis of the Venturi effect. In this design, high-pressure steam passes through a converging-diverging nozzle, accelerates and then mixes with the NCG mixture that is to be removed. As the NCG mixture becomes entrained in the motive steam flow it is pushed along with the motive steam into a diffuser. As the motive steam expands it performs work on the NCG mixture, causing it to compress and evacuate the preceding condenser. Figure 1 below shows the relative change in pressure and velocity of the motive steam and NCG mixture fluids as they pass through the SJE (7).

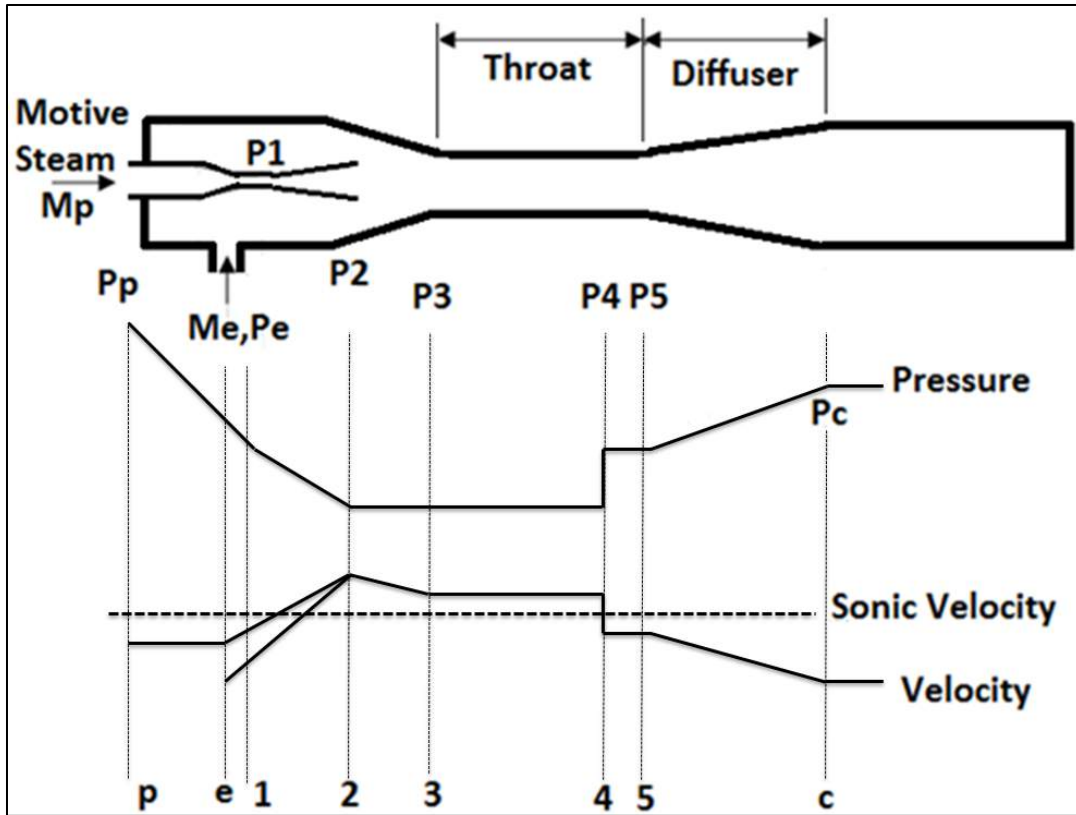


Figure 1: Fluid Pressure and Velocity Changes Through the SJE

From Figure 1 it can be seen that motive steam enters the SJE at point p with a high pressure and subsonic velocity. This motive steam then passes through a converging-diverging nozzle, reaching Mach 1 at point 1 and supersonic velocity at point 2. As the motive steam velocity accelerates its pressure decreases. Eventually the motive steam pressure is less than that of the NCG mixture. As a result, motive steam is drawn out of the suction chamber at point e. The NCG mixture and motive steam mix together as they decelerate to subsonic velocity at point 4. The fluid then passes through a diffuser to increase pressure and decrease velocity. The resultant mixture has a lower pressure than the motive steam at the inlet, but a higher pressure than the NCG at the inlet. This is because the expansion of the motive steam supplies the work

that is needed to compress the incoming NCG mixture. In general, SJE can commonly have efficiencies as low as 10 percent (4).

The key performance parameters for SJE are the Air to Steam Ratio (ASR), Expansion Ratio (ER) and Compression Ratio (CR). The ASR is the flow rate of the NCG mixture divided by the flow rate of the motive steam. Using experimental data from the Heat Exchange Institute (HEI) for SJE it is possible to determine the ASR for any mixture. This then determines the necessary motive steam consumption for a desired NCG mixture flow rate. The ER is defined as the inlet pressure of the motive steam divided by the inlet pressure of the NCG mixture. This quantifies how great the pressure ratio is between the fluid that is being moved and the fluid that is to be moved. Lastly, the CR is defined as the ratio of the SJE outlet pressure to the NCG inlet pressure. Ideally, an SJE with the highest ASR, lowest ER and required CR would define the best possible performance. The higher the NCG concentration and hence NCG flow rate, the greater the motive steam consumption necessary to drive the NCG. This motive steam, sometimes referred to as parasitic steam, reduces the possible steam supply to the turbine and thereby the turbine output. When steam is viewed as a lost revenue source this can make the operational cost of SJE systems economically infeasible, especially if the steam is entrained with a high concentration of NCG.

By far the most energy efficient means of NCG removal is turbocompression, where typical efficiencies can exceed 80 percent (4). They have been uncommonly used however due to their extremely high capital costs, several moving parts, and hence regular maintenance. The components are typically made of steel alloys that easily corrode, requiring replacement or repair. However, turbocompression provides a significant savings in operational costs when

compared with SJE, especially if there are high NCG concentrations. This is why a number of geothermal plants use centrifugal compressors in Italy (8). Turbocompressors move the NCG mixture by adding energy to the fluid through the dynamic action of blades and thereby creating a pressure difference. Many kinds of turbocompressors exist today and are broadly classified by their direction of fluid flow, which can be purely radial, diagonal or axial. They can also be steam driven or electrically driven.

In 1995 the U.S. Department of Energy awarded a grant to a turbomachinery company in Colorado, Barber-Nichols, to develop an NCG turbocompressor for the Unit 11 geothermal plant at The Geysers (9). The compressor was steam driven and was designed to provide the third and final stage of compression in a series of 2 preceding SJE. Barber Nichols says the turbocompressor can handle lower inlet pressures and larger flow rates than LRVP and therefore act as a “compact and efficient alternative to liquid-ring vacuum pumps utilized in NCG compression” (10). They claim the turbocompressor has a 30% greater efficiency than LRVP and a 250% greater efficiency than SJE. According to the Geothermal Resource Council, replacing the last stage of SJE with the Barber-Nichols compressor increased the power output of The Geysers’ Unit 11 by as much as 2 megawatts.

NCG Turbocompression in geothermal plants is rarely used elsewhere in the world, aside from Italy where NCG concentrations can exceed 10% by mass fraction (11). As a result, many Italian geothermal plants use centrifugal compressors, especially in locations where the parasitic steam losses that would be required to power SJE significantly outweigh the higher capital cost of turbocompressors. One of the largest manufacturers of these centrifugal compressor systems for geothermal plants is GE Oil & Gas (12).

In order to make turbocompressors an economic alternative to SJE at lower NCG concentrations, an axial compressor with composite impellers has been designed at Michigan State University and is intended to replace SJE that have been used for the first 2 stages of compression (13). The hub, shroud and blades of each rotor were made of a single carbon fiber filament that was wound around a mandrel and resin hardened. The single continuous fiber in each rotor was oriented so as to take advantage of the composite's high tensile strength during operation. The compressor design has 10 stages that are counter-rotating, each with permanent magnets integrated into the outer radius of the woven rotors, allowing the individual wheel to act as an independent motor drive with variable speed control. Counter-rotation reduces the necessary speed for the same work performed by traditional axial compressors and makes the design compact by eliminating stators. The direct drive motors also remove the need for a shaft to transmit torque, making each stage modular for ease of maintenance. In addition, the composite material has been found to be highly corrosion resistant. The results of the case study in this thesis are intended to provide the thermodynamic basis for the ongoing research of the woven wheel compressor at Michigan State University. Photographs of the prototype compressor and one of its composite rotors can be seen in Figure 2.



Figure 2: A Prototype Impeller of the Compressor with Integrated Magnets in the Shroud (left), and the Prototype 10 stage, Counter-Rotating, NCG Compressor (right)

## CHAPTER 2.0

### 2.1 Thermodynamic Model Assumptions for Flash Steam Geothermal Power Plants

Due to the historically high capital cost of turbocompressors, geothermal plants have rarely considered them as an alternative to SJE, especially if NCG concentrations are moderate to low. As a result, very little has been done to compare the performance of SJE and turbocompressors quantitatively in geothermal applications. In this study, a method was established and implemented to create a thermodynamic model for comparing SJE and turbocompressor gas extraction systems. The following assumptions were made in the model:

1. For simplification of the mixture analysis, the NCG is assumed to have the molecular weight of  $\text{CO}_2$ , as  $\text{CO}_2$  typically constitutes 80% or more of the NCG mixture by mass fraction (4). As a result,  $\text{CO}_2$  and NCG are synonymous in the analysis unless otherwise stated.
2. The geothermal fluid has an assumed composition of pure  $\text{H}_2\text{O}$  with  $\text{CO}_2$  dissolved in it. This is because the presence of ionic salts or other solids is typically negligible.
3. The NCG concentration passing through the turbine is assumed to be 2% by mass fraction of the total geothermal fluid.
4. The  $\text{CO}_2$  in the mixture is treated as an ideal gas, as it is sufficiently superheated throughout the geothermal system to warrant its treatment as such.
5. In the analysis of the single-flash steam plant, the steam is assumed to expand isenthalpically in the separator as the process performs no mechanical work.
6. The work of the turbine and gas extraction systems is assumed to be adiabatic.

7. The heat exchange in the condenser is assumed to be isobaric.
8. The pressure losses in pipelines between devices are assumed to be negligible.

A schematic detailing the major devices and processes in the flash plant is shown below in

Figure 3.

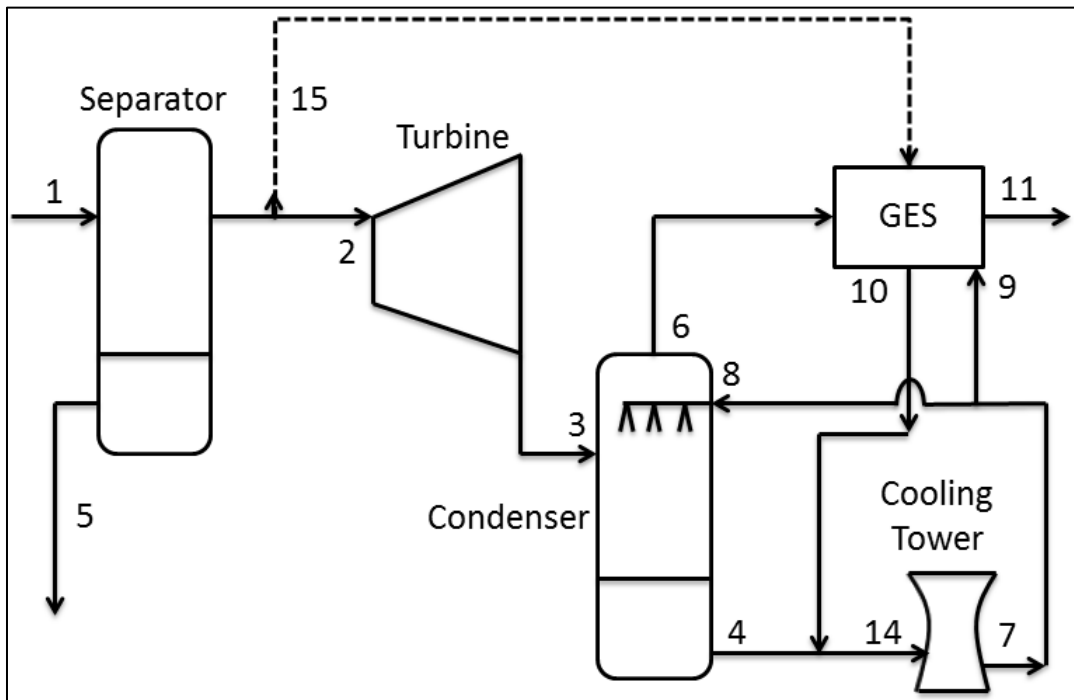


Figure 3: General Layout of a Single-Flash Power Plant

The geothermal fluid comes from the wells and enters the separator or flash tank at point 1. The vaporized portion enters the turbine as a saturated vapor at point 2, while the liquid portion, known as brine, is either reinjected to the well or used in another heat recovery process. Point 15 indicates the parasitic steam loss that would be required to drive the GES if steam jet ejectors are used. Steam exiting the turbine enters the condenser at point 3 and rejects heat to the flow of cooling water entering at point 8. A portion of the steam then condenses, exits the condenser with the cooling water at point 4 and is pumped back to the

cooling tower at point 14. The NCG does not condense in the condenser and must be evacuated to reduce the backpressure on the turbine. Whatever gas extraction system is used, there will be significant water loading in the NCG mixture leaving the condenser at point 6. Hence the mixture is sometimes referred to as wet NCG, as it can frequently contain more than 50% water vapor by mass fraction depending on the temperature of the condenser (14). This water vapor significantly increases the power consumed by the GES. For this reason serious consideration should be given to the use of a pre-cooler or even a turbochiller that can further condense the water vapor and remove it from the wet NCG. This serves the same purpose as typical inter and after condensers in the GES. After exiting the GES the wet NCG goes through H<sub>2</sub>S and Hg abatement processes before being released to the atmosphere. The processes of flashing, separating, expanding through the turbine and rejecting heat in the condenser are shown on the temperature versus entropy diagram in Figure 4.

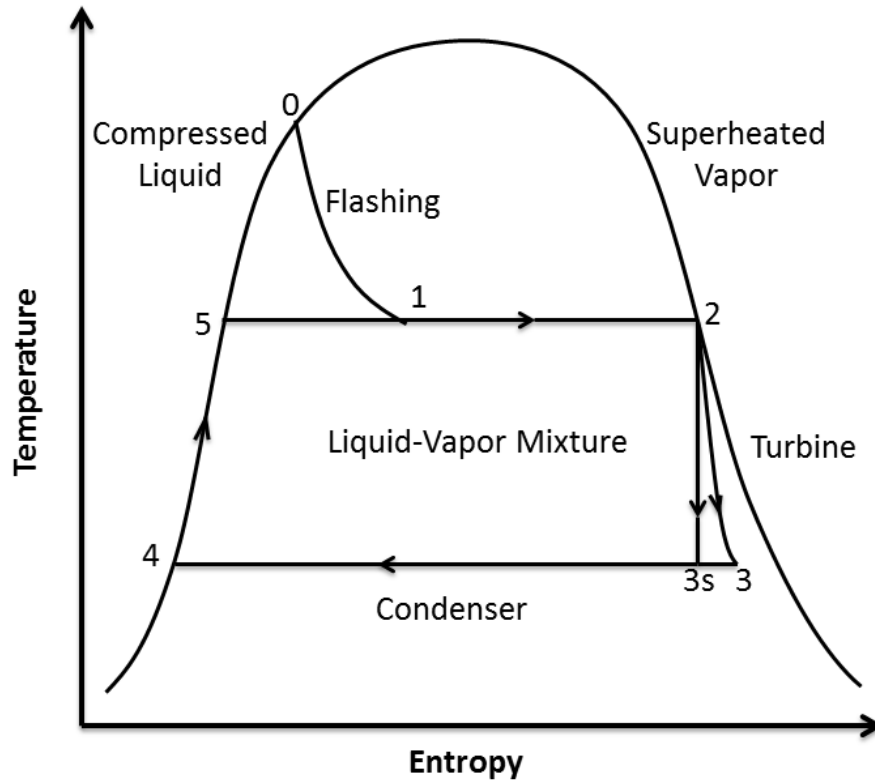


Figure 4: The Flash Plant Cycle on a Temperature-Entropy Diagram

## 2.2 Methods Used to Compare the Performance of Geothermal Gas Extraction Systems

The thermodynamic model was created using Excel and the XSteam Excel add-in functions created by Magnus Holmgren and enhanced with additional fluid properties by the University of Alabama (15). The purpose of the model is to quantitatively understand the costs and benefits of different geothermal gas extraction systems. The inputs to the model include:

1. The mass fraction of NCG present in the geothermal fluid
2. The NCG flow rate through the turbine
3. The turbine efficiency
4. The quality of steam at the inlet

5. The turbine outlet pressure, which is assumed to be equal to the condenser pressure
6. The temperature at the turbine inlet and outlet
7. The control temperature of the condenser

From these inputs, the model outputs the following data to help determine which system provides the best thermodynamic performance:

1. The motive steam consumption of the SJE necessary to evacuate the NCG load
2. The electrical energy required to power the turbocompressor system
3. The net power production of the plant using either system
4. The optimum operating pressure of the condenser for either system
5. The optimum pressures for the SJE-LRVP gas extraction system
6. The optimum pressures for the compressor-LRVP gas extraction system

Given the mass fraction defined in Equation 1 for each component in the mixture it is possible to determine the mole fraction in Equation 2. This is done by dividing the mass fraction of each mixture component by its respective molecular weight, which gives the number of moles of that component present in 1 kilogram of the mixture. Dividing the numbers of moles of a given component by the sum of moles present in the mixture yields the mole fraction as stated in Equation 2.

Equation 1: Mass Fraction Definition

$$mf_i = m_i/m_{tot}$$

Equation 2: Mole Fraction Definition

$$y_i = n_i/n_{tot}$$

Using the mole fraction of each component in the mixture it is possible to determine the molecular weight of the mixture by calculating the mole-fraction-weighted average given in Equation 3.

Equation 3: Mixture Molecular Weight

$$M = \sum_{i=1}^j y_i M_i$$

The constant pressure specific heat is defined on a molar basis for each mixture component in Equation 4. This polynomial assumes that changes in  $C_p$  are primarily temperature dependent.

The polynomial coefficients for each component in the mixture,  $CO_2$  and  $H_2O$ , are shown in Table 1 (16).

Equation 4: Specific Heat Polynomial

$$\bar{c}_p = \bar{R}(\alpha_i + \beta_i T + \gamma_i T^2 + \delta_i T^3 + \epsilon_i T^4)$$

Table 1: Coefficients of the  $C_p$  Polynomial

Gas	$\alpha$	$\beta$	$\gamma$	$\delta$	$\epsilon$
CO2	2.401	8.74E-03	-6.61E-06	2.00E-09	0
H2O	4.07	-1.11E-03	4.15E-06	-2.96E-09	8.07E-13

After finding the molar  $C_p$  of the individual components it is possible to determine the molar  $C_p$  of the mixture by calculating the mole-fraction-weighted average given in Equation 5. The mass-basis  $C_p$  can be obtained by dividing the molar  $C_p$  by the average molecular weight of the mixture.

Equation 5: Mixture Specific Heat

$$\bar{c}_{p, \text{mix}} = \sum_{i=1}^j y_i \bar{c}_{p,i}$$

The mixture gas constant,  $R_{\text{mix}}$  is found by dividing the universal molar gas constant by the average molecular weight of the mixture. The difference between the  $C_p$  of the mixture and the gas constant of the mixture will give the constant volume specific heat of the mixture,  $C_v$ , as shown in Equation 6.

Equation 6: Specific Heat Relation

$$c_{v, \text{mix}} = c_{p, \text{mix}} - R_{\text{mix}}$$

The ratio of constant pressure and constant volume specific heats can be determined according to Equation 7. This ratio of specific heats is later used in determining the mass specific work done during compression and expansion of fluids in the SJE.

Equation 7: Ratio of Specific Heats

$$\gamma_{\text{mix}} = c_{p, \text{mix}} / c_{v, \text{mix}}$$

When the steam enters the condenser, heat is rejected to the cooling water and a significant portion of the steam condenses to become a liquid. As a result, the partial pressure of the  $\text{H}_2\text{O}$  vapor in the condenser decreases. If the total pressure of the condenser is known as a controlled point, the partial pressure of  $\text{CO}_2$  can be determined from Dalton's Law of Partial Pressures given in Equation 8. This is because the partial pressure of water is known as the saturation pressure of water vapor at the control temperature of the condenser.

Equation 8: Dalton's Law of Partial Pressures

$$P = \sum_{i=1}^j P_i$$

The temperature of the condenser however is still far above the condensation temperature of CO<sub>2</sub> and other non-condensable gases. As a result, the NCG cannot be removed by the condensate pump and therefore requires a gas extraction system such as a turbocompressor or SJE. The gas extraction system must remove the NCG from the condenser at the same rate it enters the condenser in order to avoid an adverse turbine backpressure. In removing the NCG however, each gas extraction system will experience a significant amount of water loading. This water loading can be determined by relating the partial pressure of water to the mole fraction as shown in Equation 9.

Equation 9: Partial Pressure and Mole Fraction Relation

$$p_i = y_i P$$

As the water vapor load mixed with the NCG increases, the gas extraction system will consume more power or motive steam. This is why precoolers are suggested for use in any geothermal gas extraction system (14). By further condensing the wet NCG in a precooler a larger amount of the fluid can be removed by the condensate pump and the gas extraction system consumes less power or steam. Power plants should compare the cost savings that a precooler provides with the capital cost of precoolers to determine whether a precooler would warrant an acceptable return on investment in each particular case.

In order to calculate the motive steam consumption that a steam jet ejector would require for a given NCG load, it is necessary to know the temperature of the NCG as well as its

molecular weight. In 1951, the Heat Exchange Institute (HEI) sponsored numerous tests on steam jet ejectors in order to determine an empirical correlation between the NCG handling capacity of steam jet ejectors and their air handling capacity. The data from these tests was published in the HEI Standards for Steam Jet Ejectors and provides a method to graphically determine the necessary motive steam consumption for a given NCG load (17). In order to incorporate this information into the thermodynamic model, data points were selected from the HEI graphs and interpolations were performed to create functions that output the intermediate values. The graphs are used to determine a dry air equivalent mass flow rate for the wet NCG mixture that is to be compressed. Using dry air equivalent mass flow rate together with the compression and expansion ratios of the SJE, it is possible to determine the necessary motive steam consumption for a given NCG load. Figure 5 provides a 70 °F air equivalent temperature entrainment ratio for both the water vapor loading and the NCG.

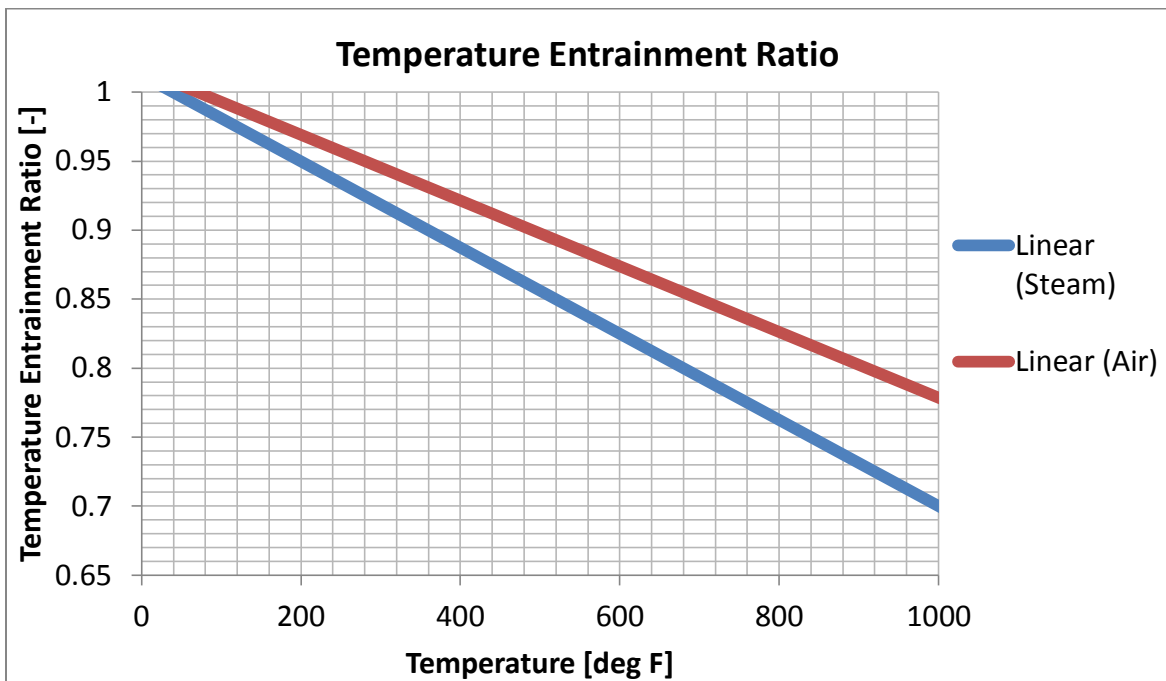


Figure 5: Temperature Entrainment Ratio Curves

The steam line in Figure 5 represents the water vapor present in the wet NCG mixture, while the air line represents the NCG. Drawing a vertical line from the wet NCG temperature given on the horizontal axis to its intersection with the steam and air lines will indicate the corresponding temperature entrainment ratio on the vertical axis for the water vapor and NCG respectively. These lines were programmed into the thermodynamic model using two data points per line from the original HEI graphs (17).

The second graph, shown in Figure 6, is used to determine the molecular weight entrainment ratio for both the water vapor load and the NCG. These values are found by drawing a vertical line from each component molecular weight on the horizontal axis to the curve. From this intersection, the corresponding molecular weight entrainment ratio for each component can be found on the vertical axis.

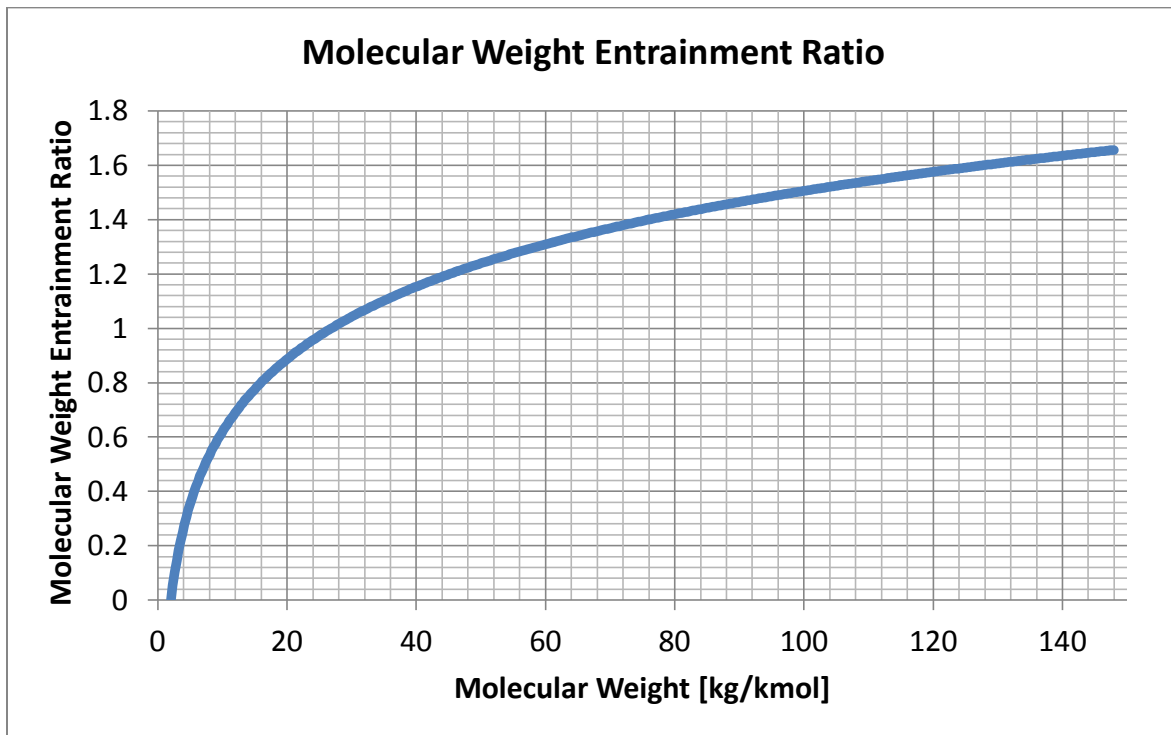


Figure 6: Molecular Weight Entrainment Ratio Curve

Assuming the wet NCG is composed of pure H<sub>2</sub>O and CO<sub>2</sub>, it is clear that these values do not change, because the component molecular weights do not change throughout the process. Using the weight entrainment ratio (WER), the temperature entrainment ratio (TER), and the mass flow rate of each component, it is possible to determine the dry air equivalent (DAE) of each component as shown in Equations 10 and 11. The DAE of the mixture can then be found as the sum of the component DAE as shown in Equation 12.

Equation 10: Dry Air Equivalent Mass Flow Rate for Steam

$$DAE_{H_2O} = \dot{m}_{H_2O} / (TER_{H_2O} WER_{H_2O})$$

Equation 11: Dry Air Equivalent Mass Flow Rate for CO<sub>2</sub>

$$DAE_{CO_2} = \dot{m}_{CO_2} / (TER_{CO_2} WER_{CO_2})$$

Equation 12: Dry Air Equivalent Mass Flow Rate for Wet NCG Mixture

$$DAE_{mix} = DAE_{CO_2} + DAE_{H_2O}$$

In order to find the required ASR for the SJE, it is necessary to define the compression ratio and expansion ratio of the fluid passing through the SJE. Equations 13 and 14 below define these ratios:

Equation 13: SJE Compression Ratio

$$CR = P_{dis} / P_{suc}$$

Equation 14: SJE Expansion Ratio

$$ER = P_{ms} / P_{suc}$$

These parameters significantly determine the performance of the SJE. A graph showing the relationship of the ER, the CR and the ASR is shown in Figure 7.

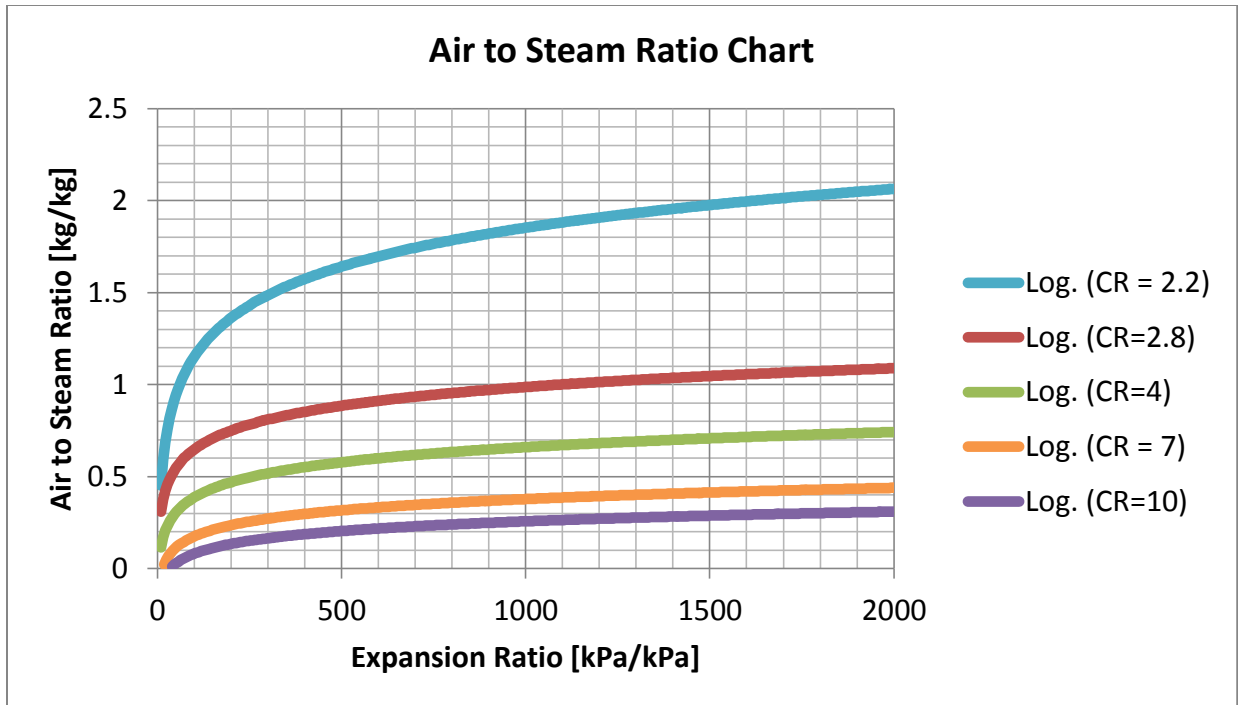


Figure 7: Relation Between Expansion Ratio, Compression Ratio, and Air to Steam Ratio

The graph of Figure 7 can be used to determine the ASR of an SJE provided that the CR and ER are known. The CR and the ER are therefore independent variables, while the ASR is the dependent variable. In order to incorporate these empirical relations from the original graph as a function in the thermodynamic model, 5 data points from each compression ratio curve were used to find an interpolation that best fit the data on the original graph. The relationship for each curve was found to be logarithmic upon graphing the original ASR data (18). The interpolated logarithmic equations were found for 3 compression ratio curves and the coefficients of each logarithmic equation were quadratically interpolated using Lagrange's form of polynomial interpolation. This quadratic interpolation of compression ratio curves provided an approximate equation for every CR curve. Because the empirical data in the original ASR graph deviated significantly from the rest of the data at low CR and low ER, the error in the quadratic interpolation of the curves increases as CR and ER values approach this range. Once

the ASR and DAE are known, it is possible to determine the motive steam consumption from Equation 15.

Equation 15: SJE Motive Steam Consumption

$$MSC = DAE_{mix} / ASR$$

The work required for an SJE to compress NCG is done by the expansion of motive steam. For the purpose of steam conservation, it is beneficial to operate at the highest possible ASR and the lowest possible DAE. However, as can be seen in Figure 7, obtaining a high ASR requires very large ER when the CR is around 2.2 or greater. This means that the best possible performance of an SJE occurs with high ER. The only way to increase ER is to either increase the motive steam pressure or decrease the condenser pressure from which the wet NCG comes. As the compression ratio increases, it is evident that the necessary increase in the expansion ratio increases exponentially if steam is to be conserved. Because the separator pressure is typically fixed, the only control variable that a plant can use to increase the expansion ratio is to decrease the condenser or precooling pressure through additional cooling.

In order to determine the thermal efficiency of the SJE it is necessary to take the ratio of the work of compression and the work of expansion performed by the SJE. This ratio defines the isentropic efficiency of the SJE and can be seen in Equation 16. Equations 17 and 18 define the work done by compression and expansion (19).

Equation 16: Isentropic Efficiency of the SJE

$$\eta_{is} = (ASR \tilde{e}_{is,comp}) / \tilde{e}_{is,expan}$$

Equation 17: SJE Mass Specific Work of Compression

$$\tilde{e}_{is,comp} = c_p T_{R1} [(CR)^{\gamma-1} / \gamma - 1]$$

Equation 18: SJE Mass Specific Work of Expansion

$$\tilde{e}_{is,expan} = c_p T_{R1} [(ER/CR)^{(\gamma-1)/\gamma} - 1]$$

Equation 19 provides a relationship whereby the polytropic efficiency can be found from the isentropic efficiency, specific heat ratio and the compression ratio (20).

Equation 19: Isentropic and Polytropic Efficiency Relation

$$\eta_{is} = \left[ \left( \frac{P_{dis}}{P_{suc}} \right)^{(\gamma-1)/\gamma} - 1 \right] / \left[ \left( \frac{P_{dis}}{P_{suc}} \right)^{(\gamma-1)/(\eta_{poly}\gamma)} - 1 \right]$$

In this study the SJE efficiency at different operating conditions was compared with the effective efficiency of a turbocompressor at the same operating conditions. In order to compare the SJE and turbocompressor systems, the effective efficiency was defined as the product of the efficiencies in the generator, the transmission, the variable frequency drive, the electrical motor and the turbocompressor.

To determine the power consumed by each gas extraction system it is necessary to define the mass flow rates and enthalpies at the inlet and the outlet of each device. From Equation 20 it is clear that the power consumption of either gas extraction system increases when the wet NCG mass flow rate increases or enthalpy change increases.

Equation 20: Power Consumption of the Gas Extraction System

$$P_{GES} = [\dot{m}(h_{2,mix} - h_{1,mix})] / \eta_{GES}$$

These mixture enthalpies on a molar basis are determined using Equation 21.

Equation 21: Mixture Enthalpy

$$\bar{h}_{mix} = \sum_{i=1}^j n_i \bar{h}_i(T)$$

For the case of the SJE, there are two inlets for mass flow, each with different mole fractions and a single outlet. For wet NCG entering the SJE, the mole fraction was determined from Dalton's law of partial pressures. For the motive steam entering the SJE the mole fraction was assumed to be equal to the mole fraction entering the turbine. This is because the mixture composition leaving the separator remains the same whether it is sent to the turbine or used to drive the SJE. Both incoming mass flow rates are used to find the total enthalpy entering the SJE. The enthalpy of CO<sub>2</sub> in the mixture was found by an ideal gas assumption, such that it was equal to the product of Cp and temperature as shown in Equation 22.

Equation 22: Ideal Gas Enthalpy Approximation

$$\bar{h}_{\text{CO}_2} = c_{P,\text{CO}_2} T$$

The enthalpy of the H<sub>2</sub>O was found from the partial pressure of H<sub>2</sub>O and the assumption of constant entropy across the device. The molar entropy of the mixture at both inlet and outlet was found using Equation 23. To find the mass-basis entropy, the molar entropy was divided by the mixture molecular weight.

Equation 23: Mixture Entropy

$$\bar{s}_{\text{mix}} = \sum_{i=1}^j n_i \bar{s}_i(T, p_i)$$

Finally, the net power of the plant was defined as the difference of the power generated by the turbine and the power consumed by either the compressor or SJE and the liquid ring vacuum pump as shown in Equation 24.

Equation 24: Net Power Output

$$P_{\text{net}} = P_{\text{turb}} - P_{\text{GES}} - P_{\text{LRVP}}$$

It should be noted that this equation neglects the additional power consumption required by the condensate pumps and the cooling tower.

## CHAPTER 3.0

### 3.1 Case Study of a Typical Flash Steam Plant

In this study a geothermal flash steam plant was modeled and its thermodynamic performance was analyzed for two different NCG removal systems. The first system was a set of 2 SJE followed by an LRVP and the second system was a turbocompressor followed by an LRVP. It is intended that this study would provide the thermodynamic basis to support the ongoing research of the Michigan State University patented woven wheel compressor technology invented by Dr. Norbert Mueller. The current compressor prototype is a 10 stage axial turbocompressor that is intended to replace two SJE in the first stages of compression. It is then followed by an LRVP. Despite proper reinjection efforts many geothermal plants are concerned with the rate of steam depletion in their geothermal fields and as such they are considering turbocompression technology to find a more steam efficient means of NCG removal than traditional SJE. The woven wheel compressor is intended to meet this need at a capital cost that is competitive with industry alternatives.

In replacing these two SJE with a single axial compressor, it is important to find the optimum operating pressure of the condenser for a given temperature that produces the greatest net power for the power plant. The optimum condenser pressure is not the same for both the SJE and compressor systems at the same temperature. Because LRVP are more efficient than SJE, the optimum condenser pressure in the SJE system will be one in which compression of the LRVP is maximized. The operational limit for LRVP is typically the inlet pressure, which cannot go below the saturation pressure of water if its ring is made of water. This means that the best operating scheme for a hybrid SJE and LRVP system is to fix the outlet

pressure of the SJE, such that the LRVP operates at a constant pressure ratio. Holding the SJE outlet pressure to a fixed value corresponding to the lower limit of the LRVP is referred to as Case 1 in this analysis. The effect that such an operating scheme has on a hybrid system consisting of a compressor and LRVP system is also analyzed and compared.

In a compressor-LRVP hybrid system, forcing the compressor to provide the maximum pressure ratio is the more efficient operational scheme for a hybrid system consisting of a compressor and LRVP. This is because mechanical compressors have typical efficiencies that exceed those of LRVP. As a result, it is desirable to accomplish as much compression as possible through the compressor and leave the remaining compression for the LRVP. In this scheme the compressor has a constant pressure ratio, but varying outlet pressure. This is referred to as Case 2 in the following analysis. The effect that such an operating scheme has on a hybrid system consisting of an SJE and LRVP system is also analyzed and compared. A comparison of typical operating pressures in a geothermal gas extraction system is shown in Figure 8. For brevity, the symbol WW is hereinafter used as an abbreviation for the MSU patented woven wheel compressor. However the thermodynamic results presented apply to compressors in general and are not peculiar to the woven wheel compressor.

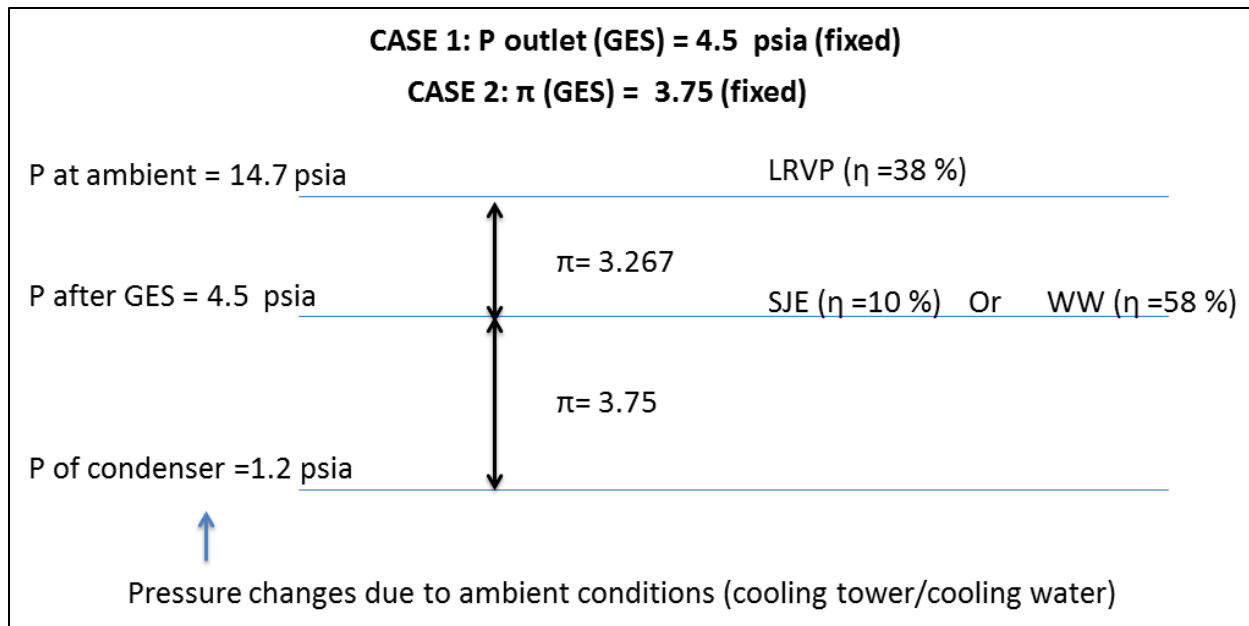


Figure 8: Typical Operational Pressures in a Geothermal GES

The inlet pressure to either gas extraction system varies according to the temperature of the condenser. Finding the optimum condenser pressure for either gas extraction system is important to maximize the net power production of the plant. Therefore, a range of optimum condenser operating pressures was found for the SJE and compressor hybrid systems in Cases 1 and 2. By optimum condenser operating pressure, it is meant as the pressure of the condenser that provides the largest possible net power output for the plant at a given condenser outlet temperature. To find this optimum pressure versus temperature relation for Case 1 and Case 2, a condenser outlet temperature was selected and held constant while varying the condenser pressure. The condenser pressure that corresponded to the highest power output for the plant at that temperature was then defined as an optimum pressure for that selected temperature. This was repeated 6 times for each case over a broad range of possible condenser temperatures. Figures 25 through 36 in the appendix show these results graphically. From these graphs it is evident that operating slightly above the optimum condenser pressure has

little effect on the net power production when compared to the drastic decrease in power production that occurs when operating slightly below the optimum pressure.

The optimum condenser pressures at each of the selected temperatures were then plotted on a pressure versus temperature diagram. A quadratic interpolation of each curve was then used to find a general equation relating the optimum condenser pressure to the condenser temperature. Figures 9 and 10 show the results of these pressure-temperature diagrams for Case 1 and Case 2 respectively. It is evident from these diagrams that the optimum operating pressure of the condenser is lower for a hybrid compressor system than for a hybrid SJE system.

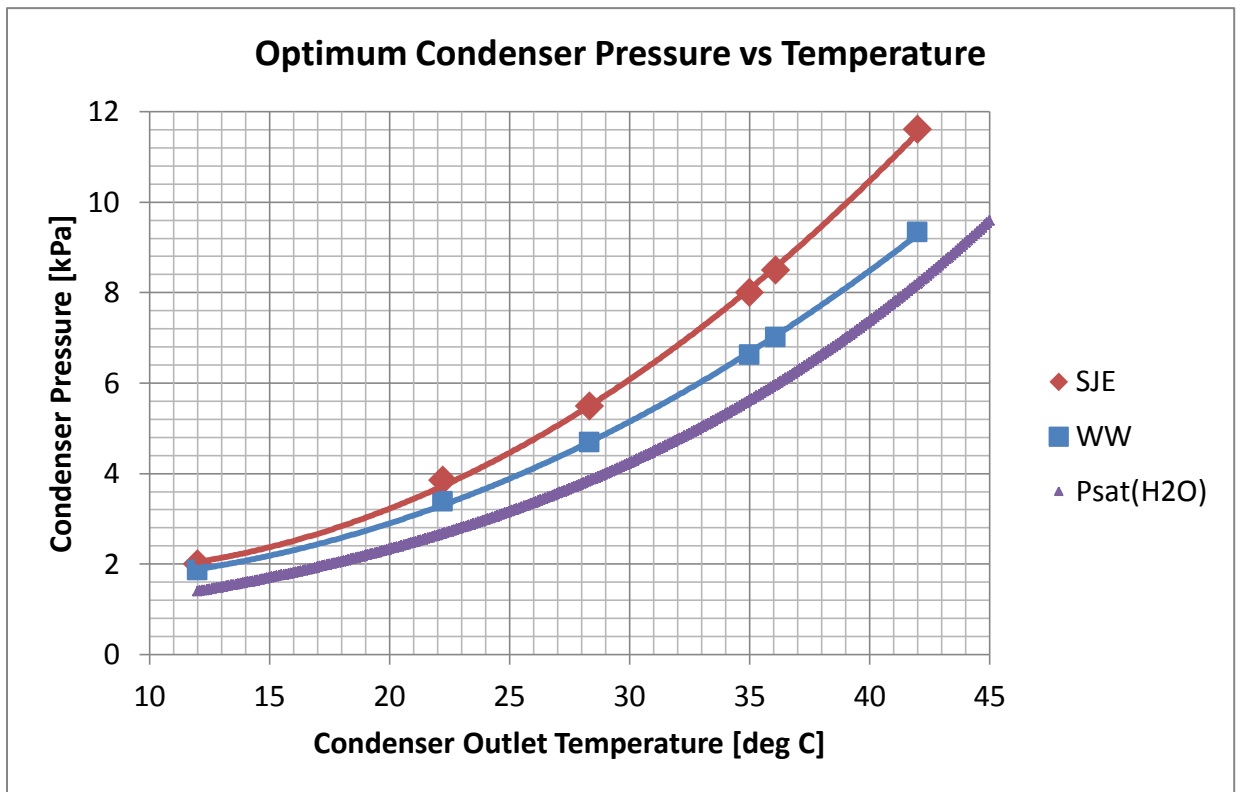


Figure 9: Optimum Condenser Pressure Diagram for Case 1

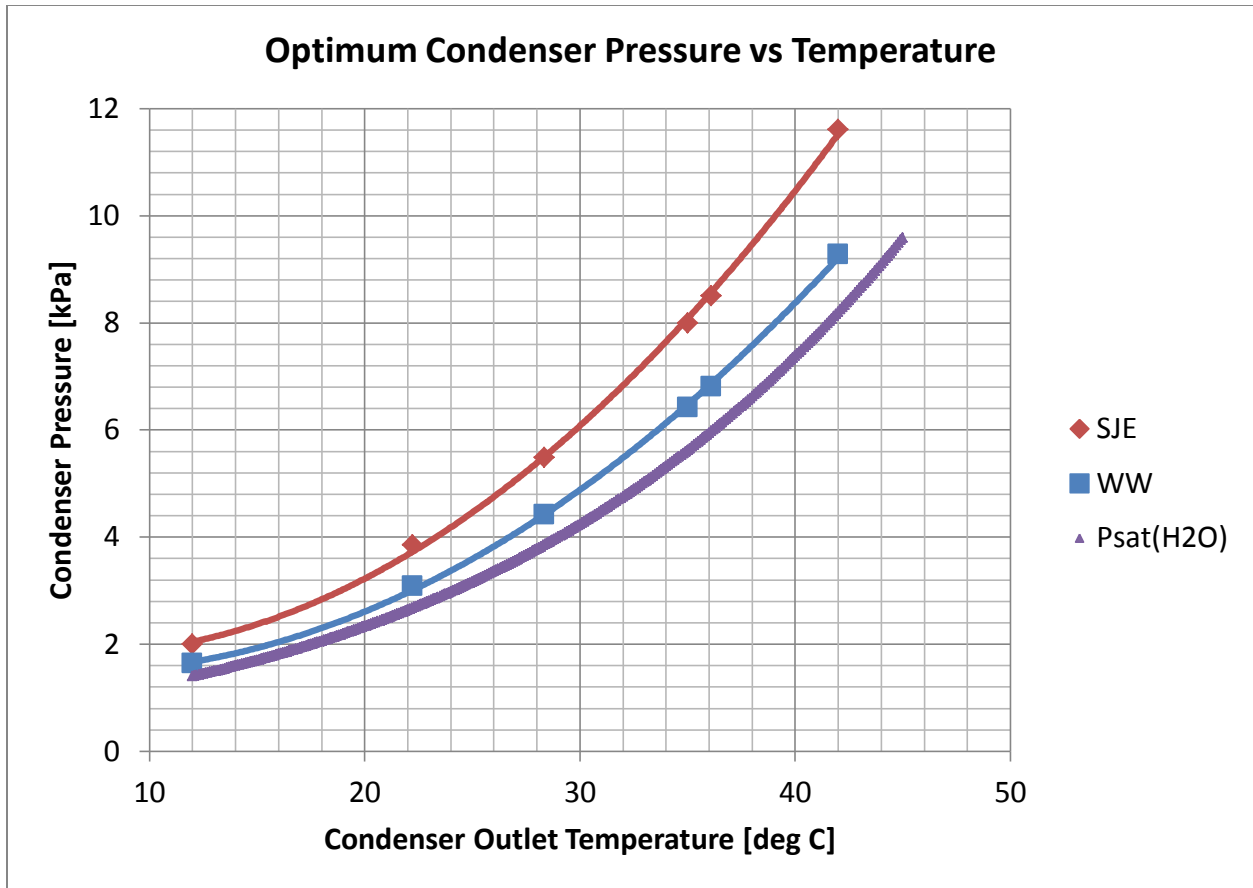


Figure 10: Optimum Condenser Pressure Diagram for Case 2

From the quadratic interpolation equations shown in Figures 9 and 10, it was possible to find the optimum condenser pressure at any given condenser temperature. This was done for both cases over a broad temperature range. Using the interpolated optimum pressure equations, the net power production of the plant for both cases was plotted against condenser temperature. This can be seen in Figures 11 and 12 for Case 1 and Case 2 respectively.

Comparing only the SJE systems in either case, it is evident from these figures that the plant with the SJE system in Case 1 has the greatest net power production, where the SJE outlet pressure is fixed to the LRVP's lower pressure limit. It is also evident that the plant with the

compressor system has the greatest net power production in Case 2, in which the compressor pressure ratio is fixed to its maximum operational point.

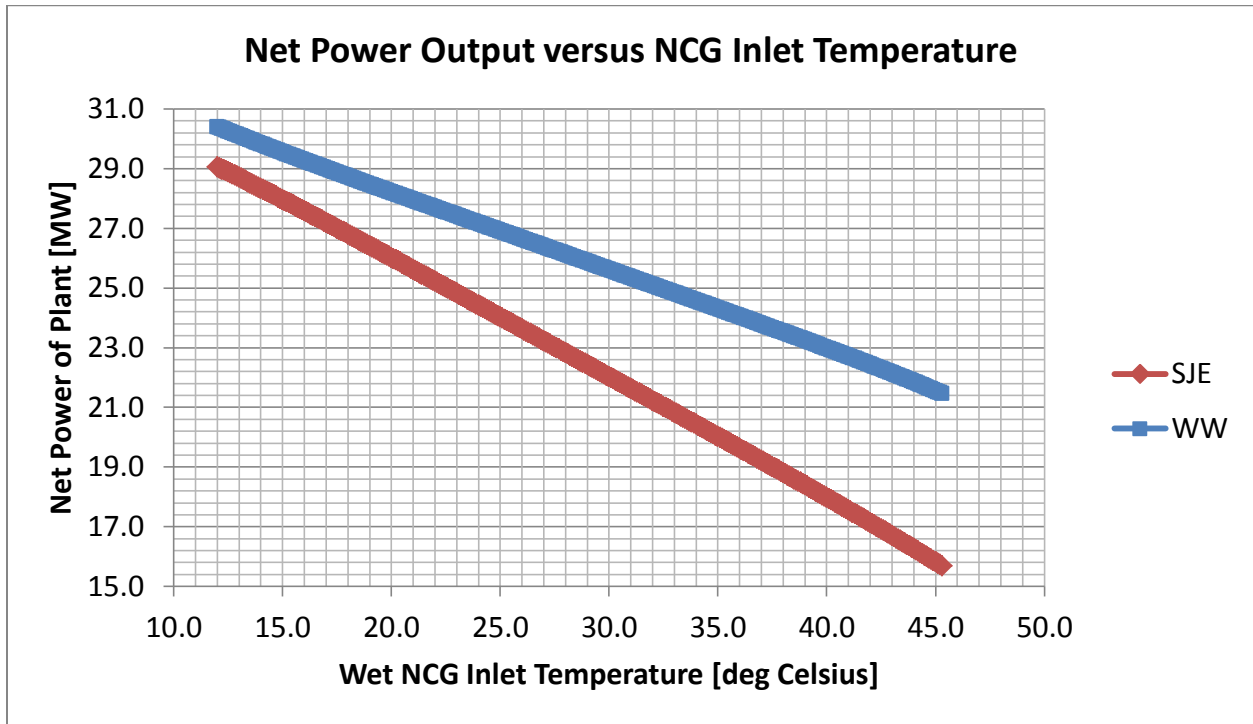


Figure 11: Net Power Output Diagram for Case 1

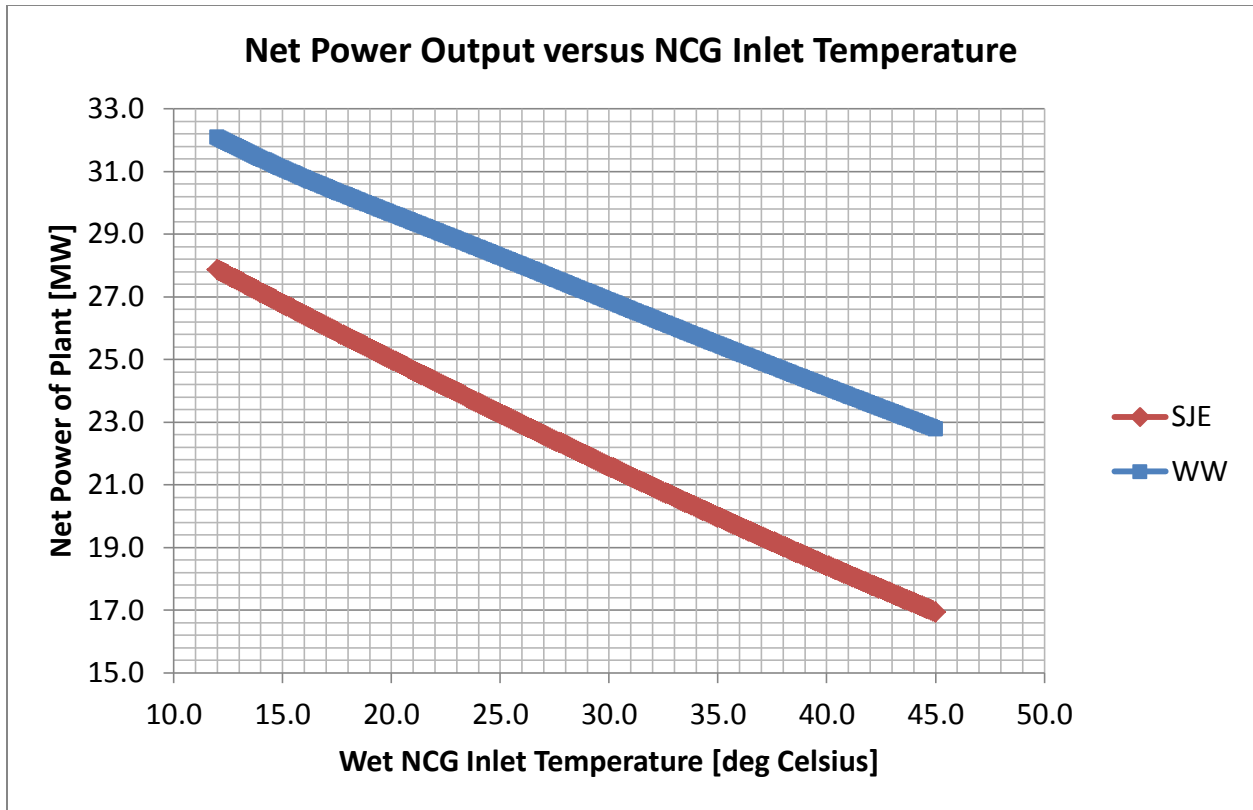


Figure 12: Net Power Output Diagram for Case 2

The power consumption of the compressor and SJE was also plotted against the condenser outlet temperature. Figures 13 and 14 show the power consumption for both Case 1 and Case 2. It is evident from these figures that the power consumption of the SJE is least in Case 1 and that the power consumption of the compressor is least in Case 2. The six critical points where optimum pressure-temperature relations were found are shown in bold, while the values from the quadratic pressure interpolation are shown as a thin line. It can be observed that the power consumption for the compressor system decreases in Case 1, but increases in Case 2. Since power is defined as the product of mass flow rate and mass specific shaft work, two factors account for this behavior. The mass flow rate always increases with increasing temperature due to increased water loading in the NCG fluid that is being compressed.

However, in Case 1, where the compressor outlet pressure is fixed, the pressure ratio decreases as the inlet temperature and inlet pressure increase. This decreasing pressure ratio for the compressor in Case 1 is so significant that it outweighs the greater mass flow at higher temperatures and hence the power consumption actually decreases with increasing inlet temperature.

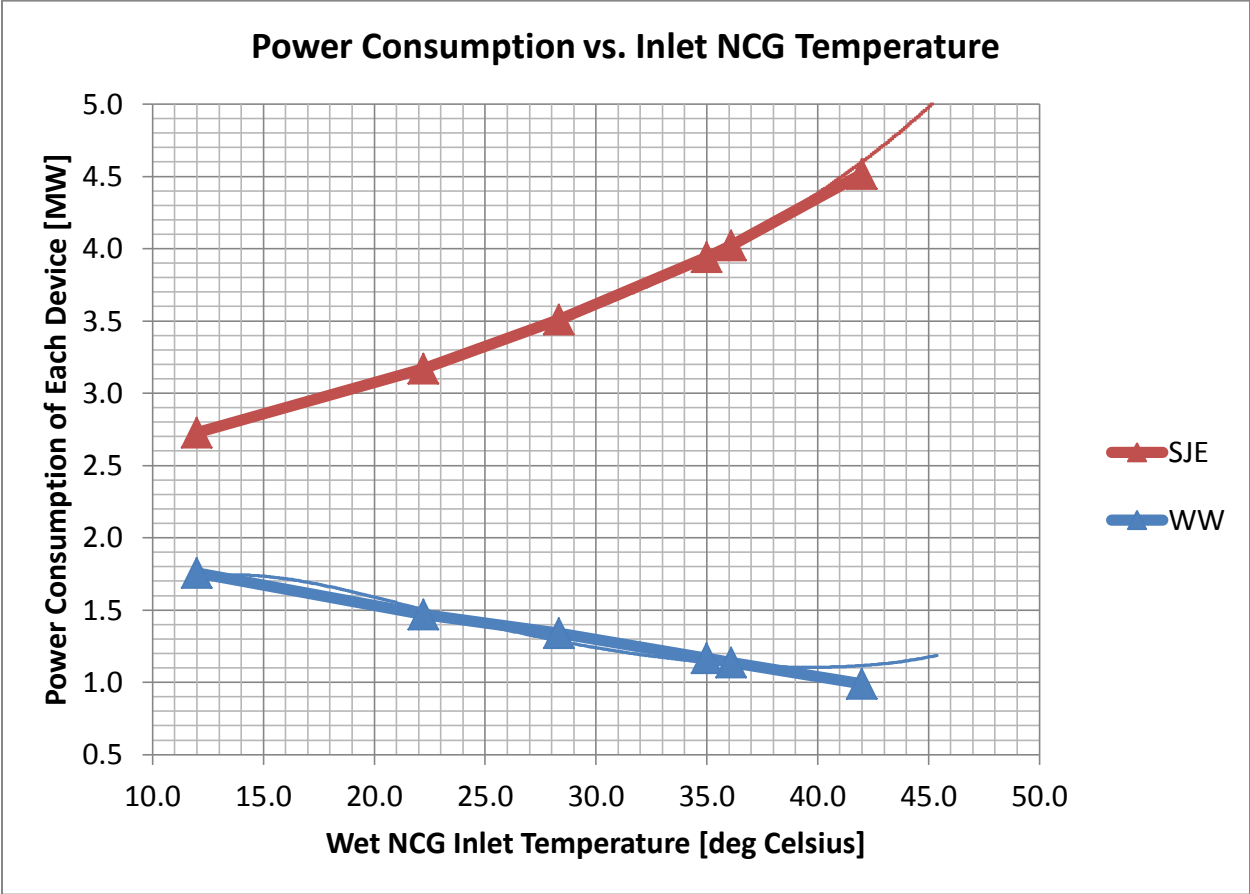


Figure 13: Power Consumption for Case 1

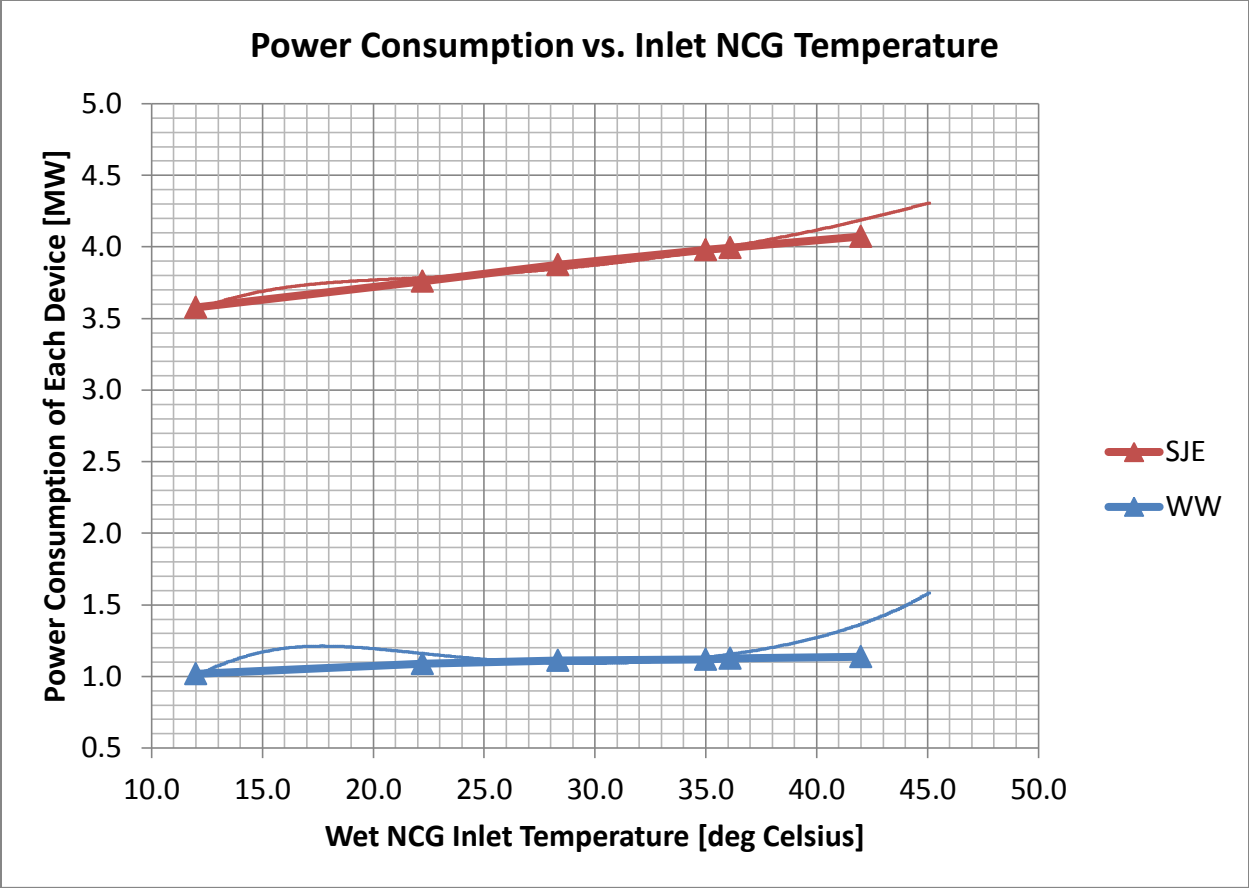


Figure 14: Power Consumption for Case 2

The difference in net power production between the SJE and the compressor systems was plotted in Figures 15 and 16 for Case 1 and Case 2 respectively. From the previous data it is evident that the SJE system has the best performance in Case 1 and that the compressor system has the best performance in Case 2. As a result, the comparison of SJE and compressor systems in Case 1 show the difference in net power production when the SJE is operating at its optimum performance and the compressor is not. Likewise, the comparison of SJE and compressor systems in Case 2 show the difference in net power production when the compressor is operating at its optimum performance and the SJE is not.

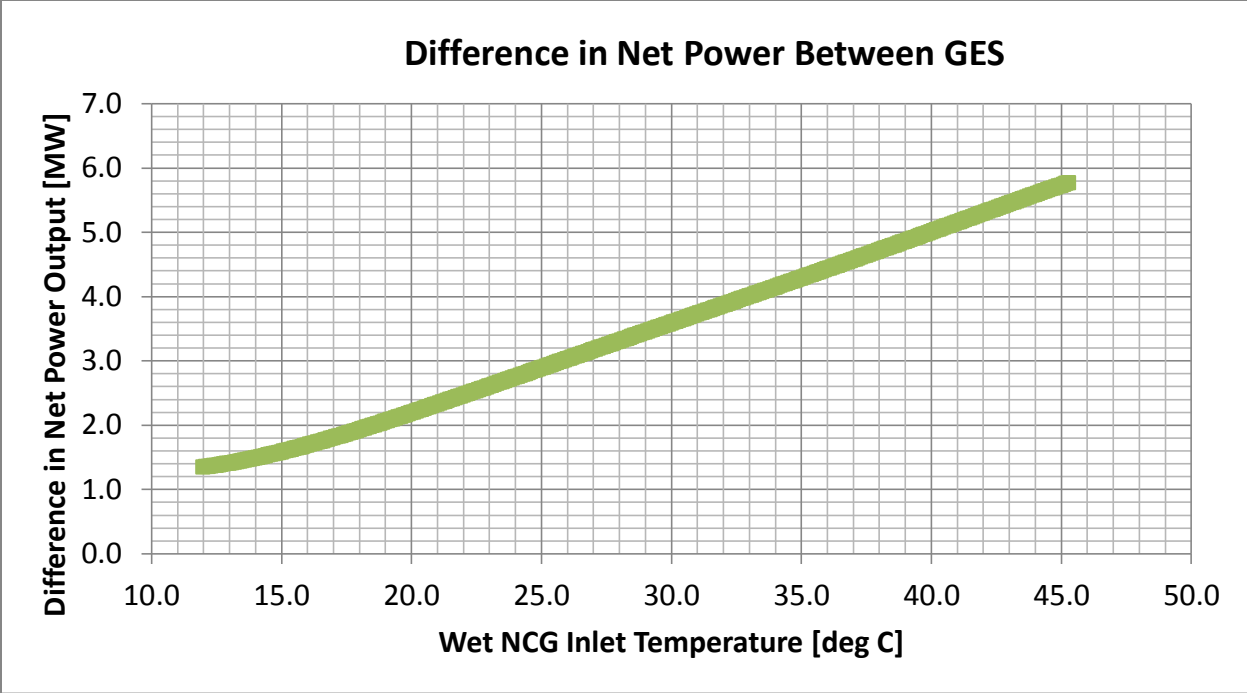


Figure 15: Difference in Net Power Output for Case 1

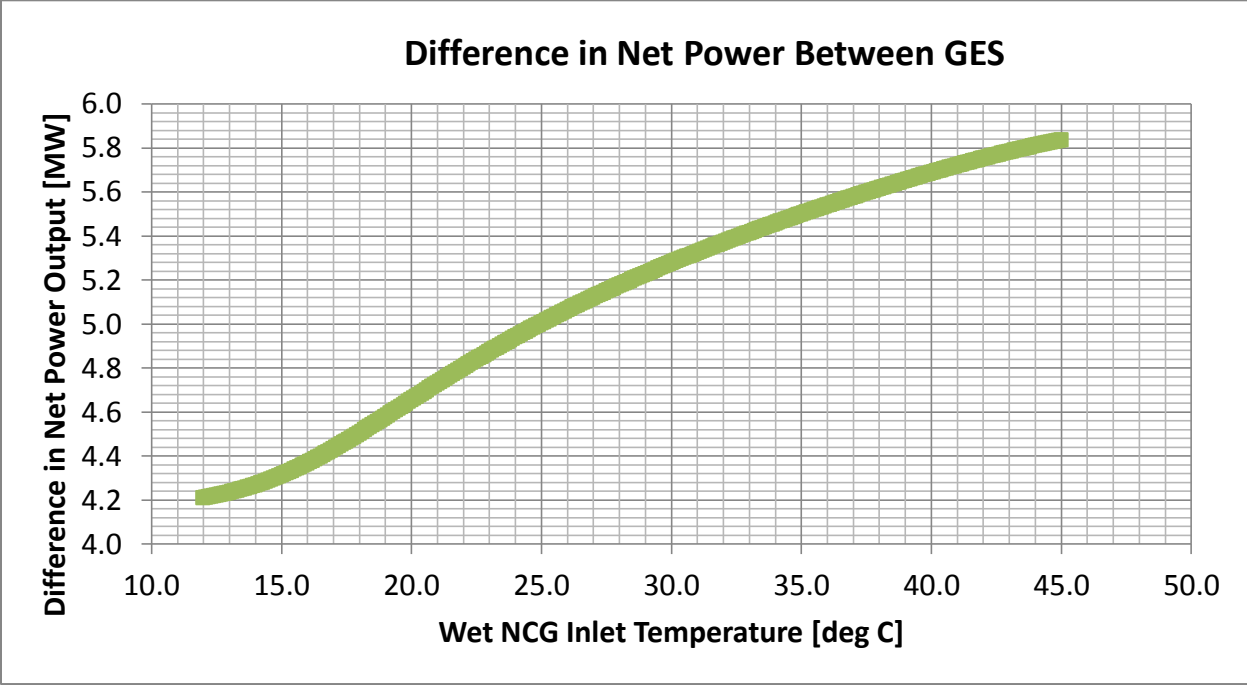


Figure 16: Difference in Net Power Output for Case 2

The change in specific heat for the SJE and compressor systems was also plotted against the condenser outlet temperature. This is shown in Figures 17 and 18 for Case 1 and Case 2 respectively. It is evident from these figures that the increase of specific heat with respect to temperature in Case 2 is significantly greater than in Case 1, even though the specific heats are lower in Case 2.

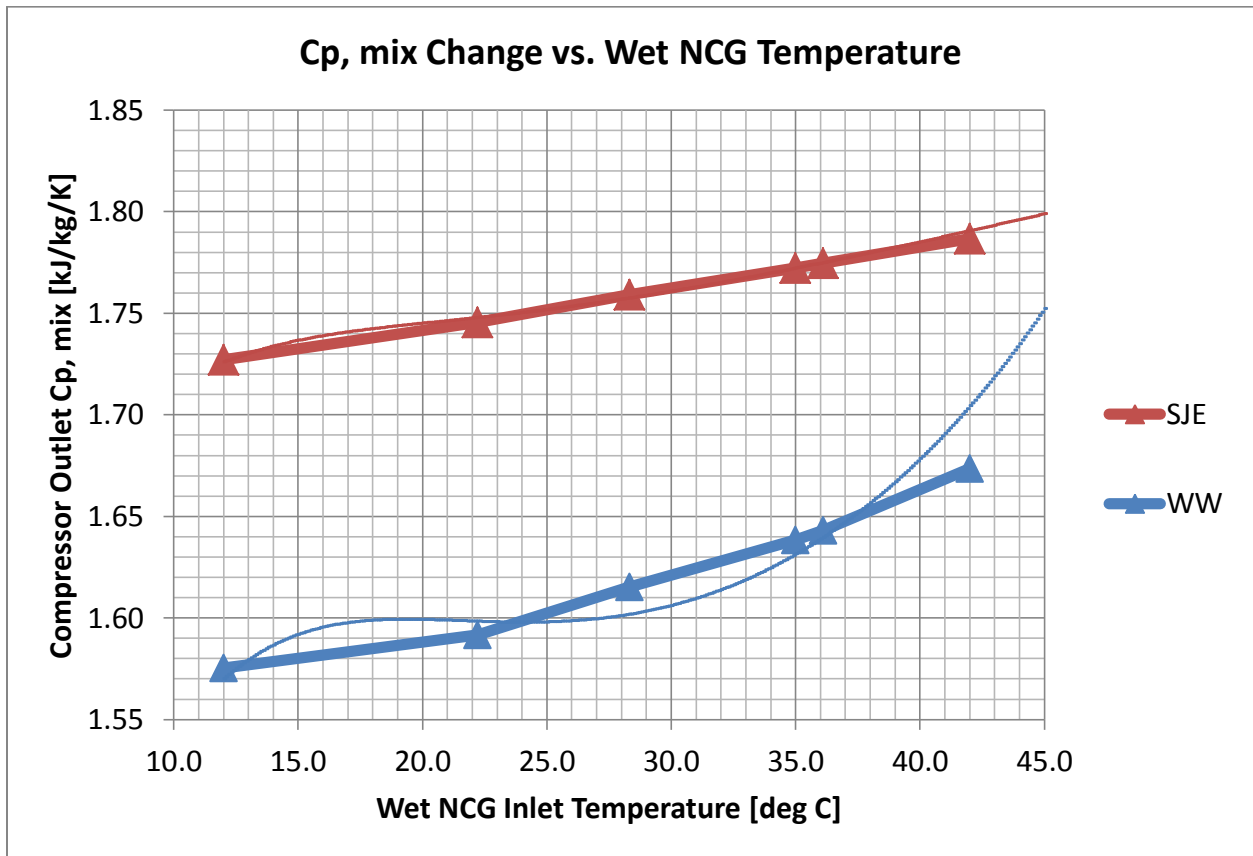


Figure 17: Change in Specific Heat for Case 1

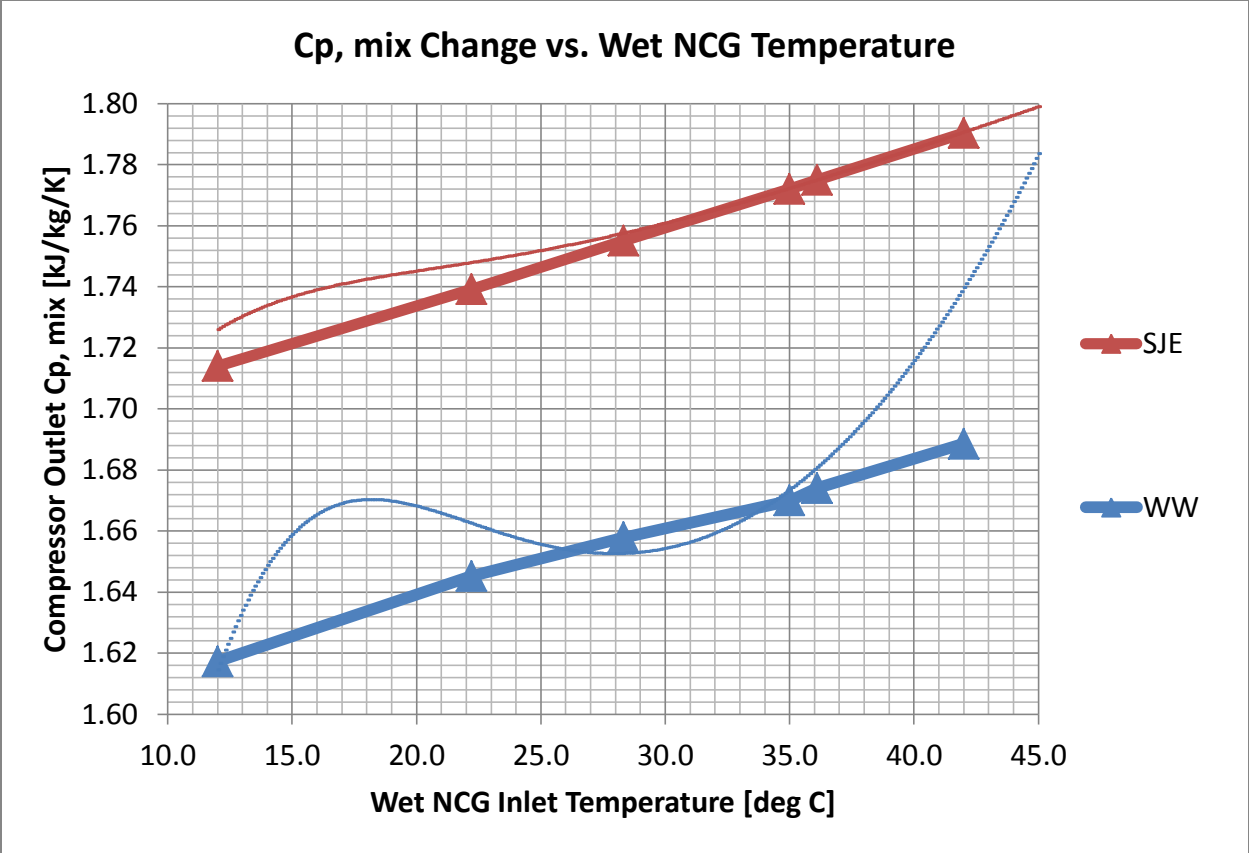


Figure 18: Change in Specific Heat for Case 2

The change in mass flow rate for the SJE and compressor systems was also plotted against the condenser outlet temperature. This is shown in Figures 19 and 20 for Case 1 and Case 2 respectively. It is evident from these figures that the mass flow rate for the compressor system is significantly greater in Case 2 than in Case 1 and only marginally greater for the SJE system. This SJE behavior can be accounted for due to the increase in motive steam required to drive the compressor at higher NCG flow rates. As the motive steam consumption increases with increasing NCG temperature, the total steam supplied to the turbine decreases and therefore the NCG load also decreases.

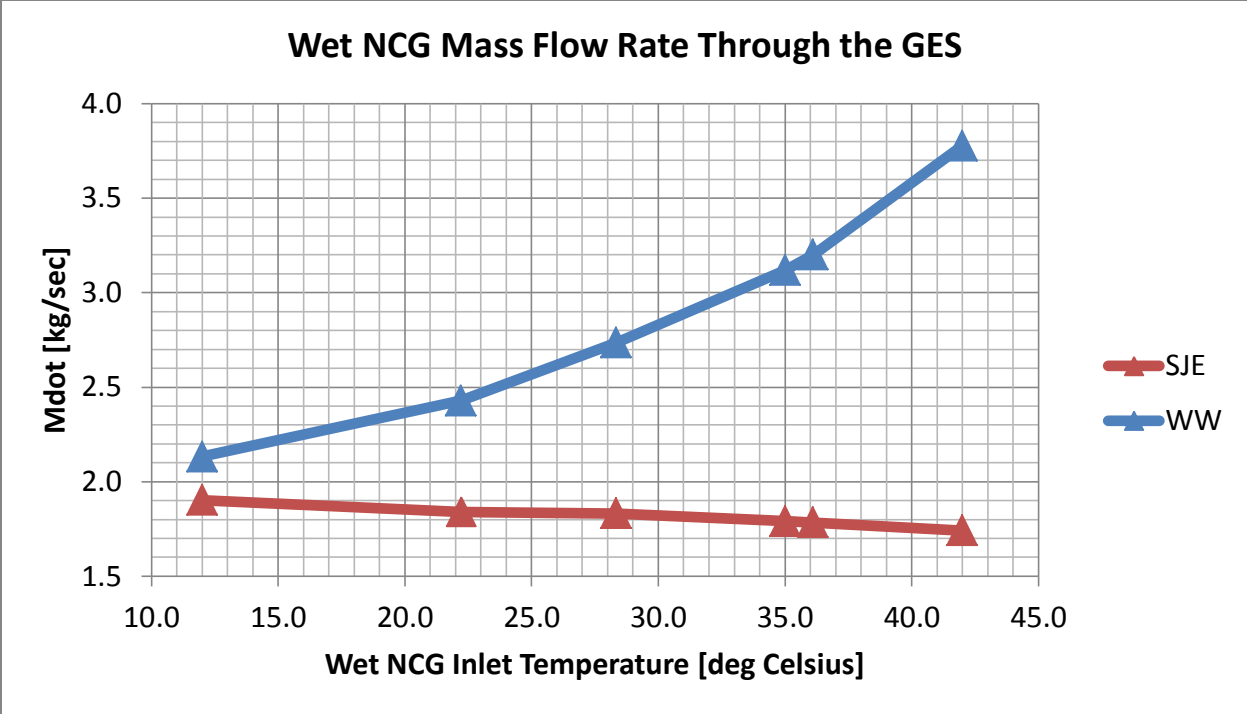


Figure 19: Mass Flow Rates for Case 1

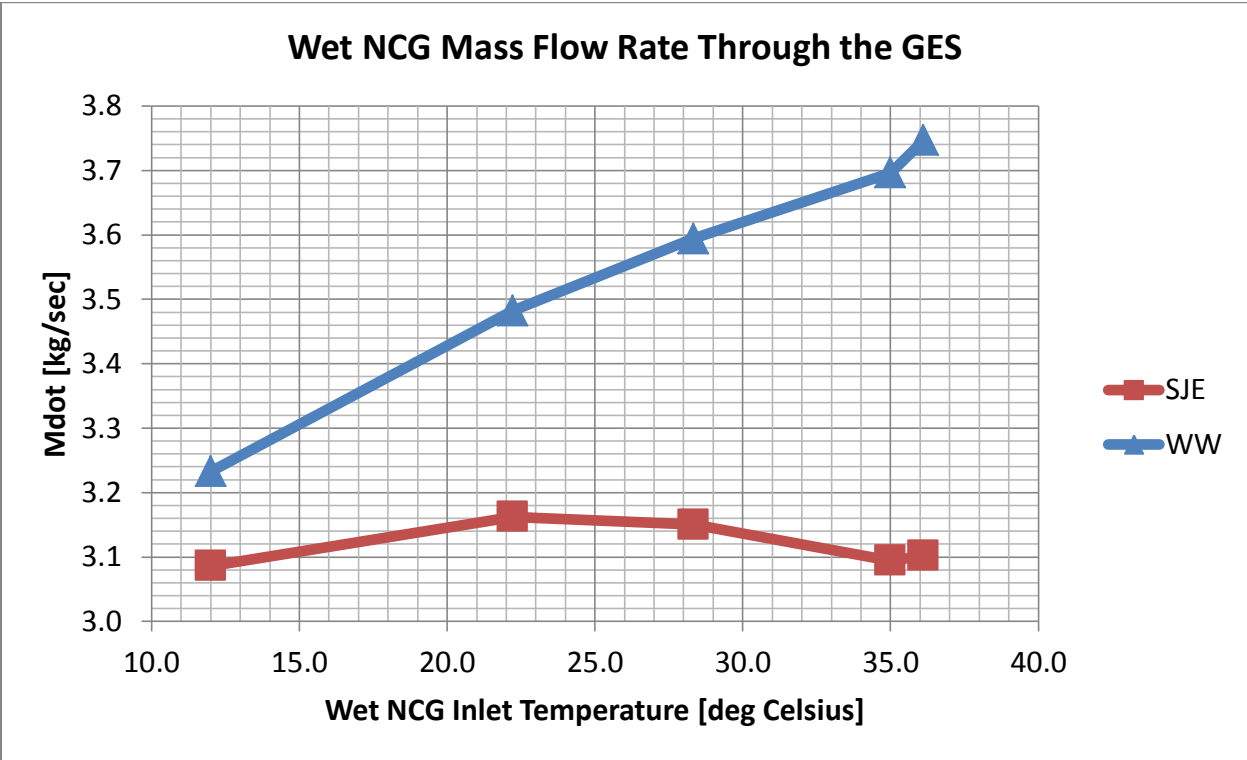


Figure 20: Mass Flow Rates for Case 2

The change in outlet temperature for the SJE and compressor was also plotted against the condenser outlet temperature. This is shown in Figures 21 and 22 for Case 1 and Case 2 respectively. Most evident from these figures is the fact that the compressor outlet temperature decreases with increasing inlet temperature in Case1, but increases with increasing inlet temperature in Case 2. The SJE outlet temperature on the other hand increases in both cases with increasing inlet temperature.

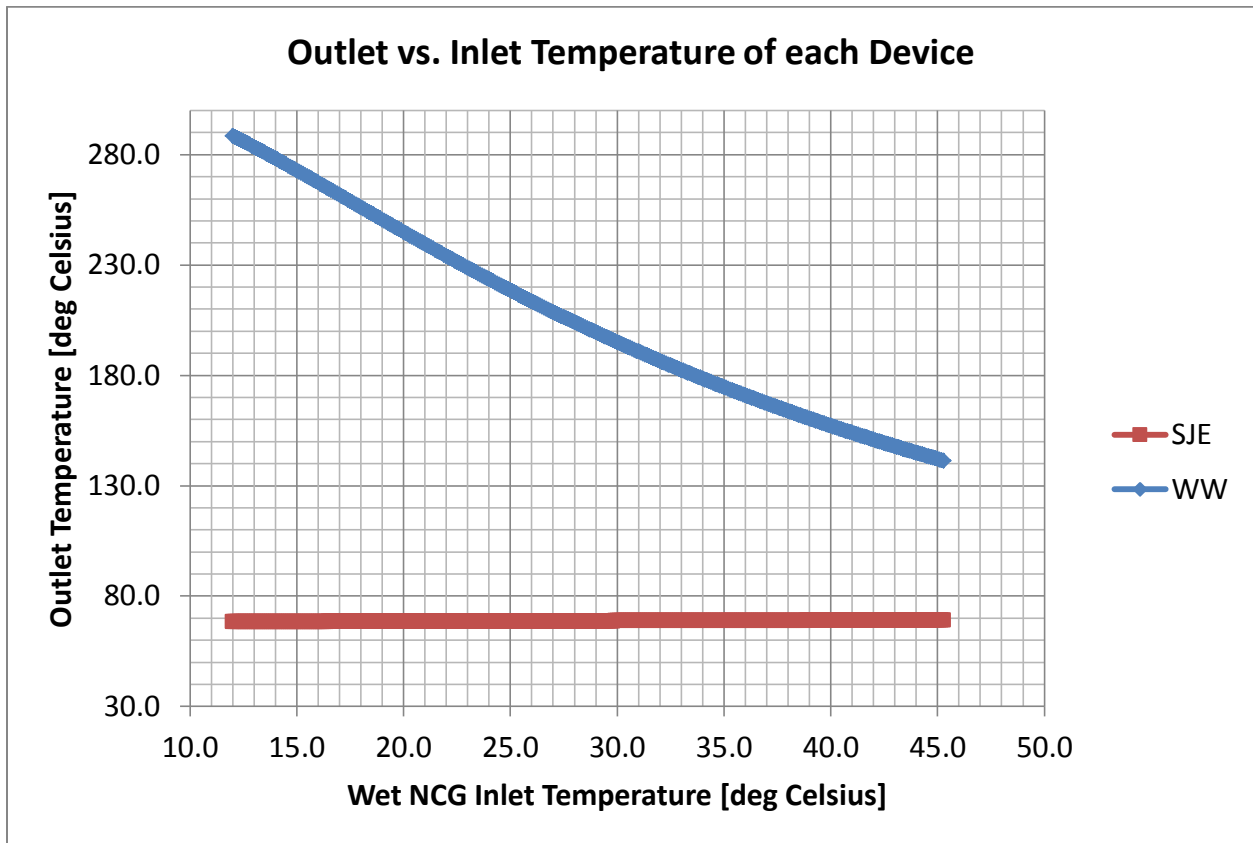


Figure 21: Outlet Temperatures for Case 1

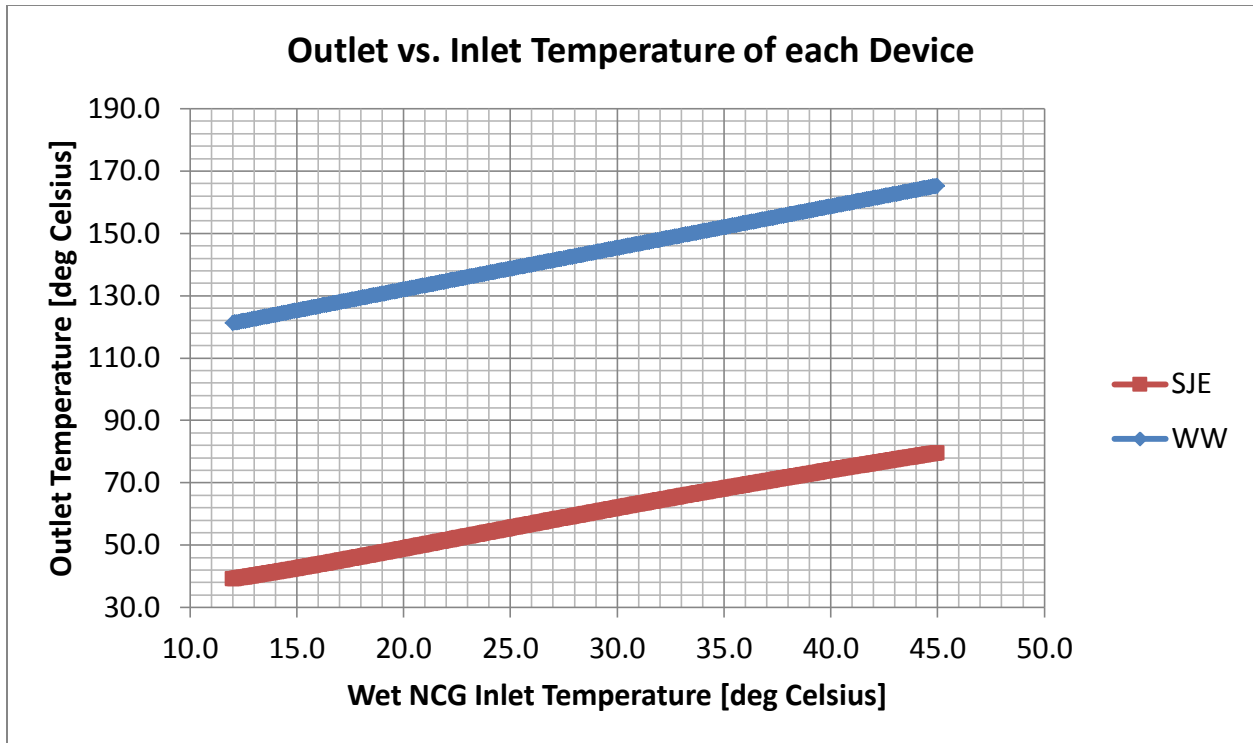


Figure 22: Outlet Temperatures for Case 2

Finally, the change in molecular weight was plotted against the condenser outlet temperature. This is shown in Figures 23 and 24 for Case 1 and Case 2 respectively. It is evident from these figures that the mixture molecular weight of the wet NCG is significantly greater in Case 1 than in Case 2, especially at lower inlet temperatures. The higher molecular weight corresponds to a higher mole fraction of  $\text{CO}_2$  and the lower the molecular weight corresponds to a higher mole fraction of water vapor. From these graphs, it is clear at any given temperature that the water loading is greater in Case 2 than in Case 1.

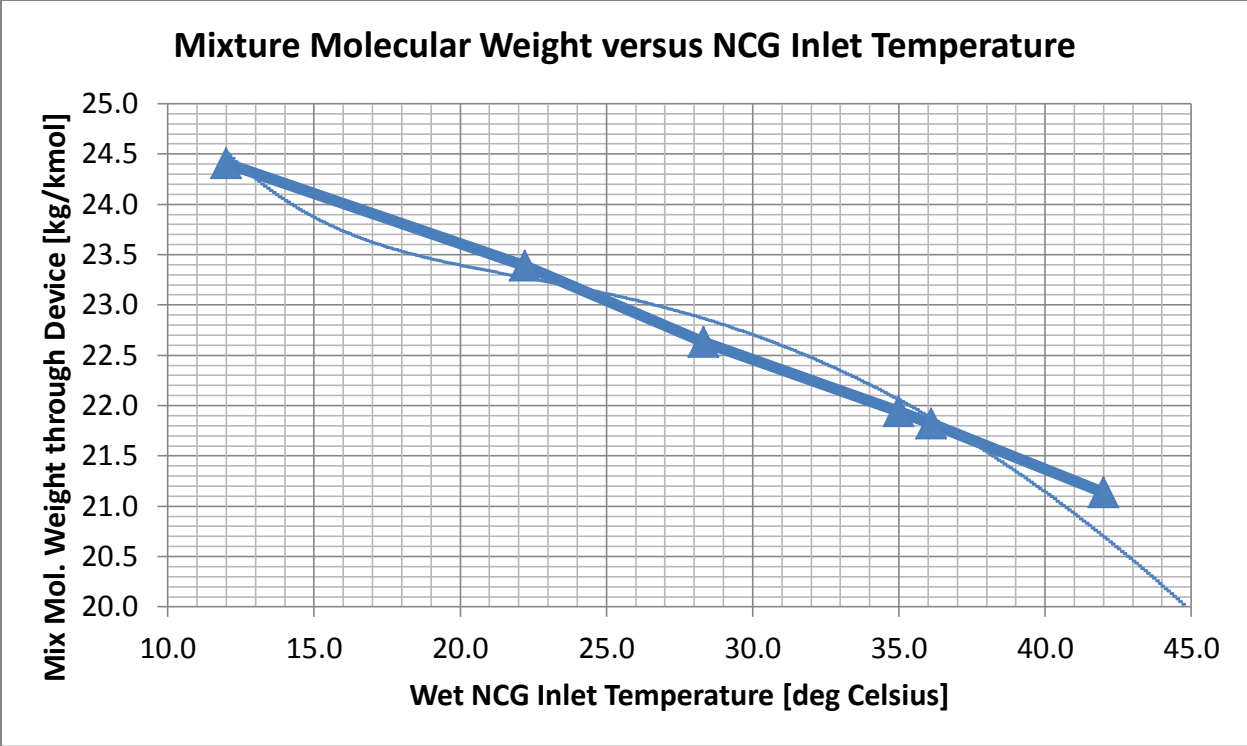


Figure 23: Mixture Molecular Weight for Case 1

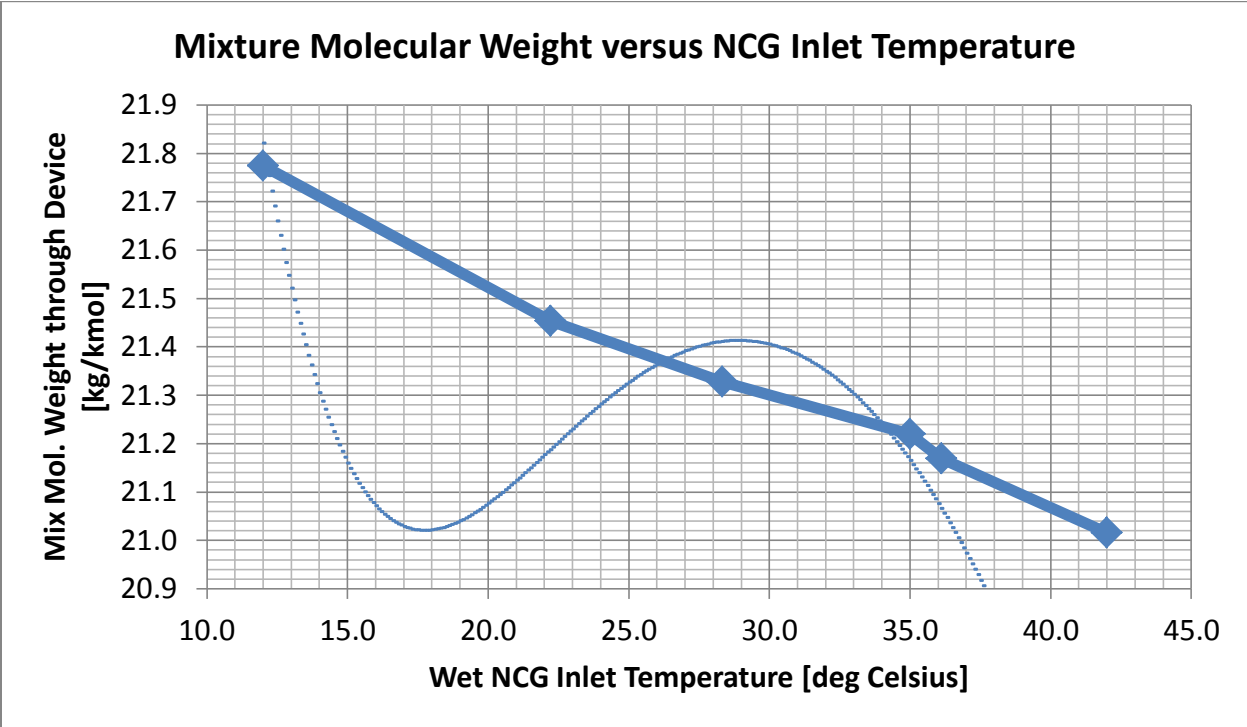


Figure 24: Mixture Molecular Weight for Case 2

## CHAPTER 4.0

### 4.1 Conclusions

From the thermodynamic analysis shown in the previous chapter, it is clear that turbocompression for NCG removal increases the net power production of a geothermal plant for both operating cases examined. The two cases show however that a geothermal power plant should not follow the same operating principles regardless of the gas extraction system chosen. This is particularly important as more and more geothermal plants consider retrofitting existing SJE systems with more efficient compressor systems.

Case 1 was chosen as the conventional operating principle in geothermal plants for traditional SJE systems, where the outlet pressure is fixed to the lower pressure limit of the subsequent LRVP. This is not without good reason, as it maximizes the compression work done by the more efficient LRVP and minimizes the work done by the less efficient SJE. The thermodynamic model created for this analysis has shown that retrofitting such an SJE system with a compressor would increase the net power production of the plant even if the same operational principles were used. However, to truly realize the full benefit of NCG turbocompression, plant operators should ensure that the compressor is operating near its maximum pressure ratio and fix it as such. This is Case 2. By accomplishing as much compression as possible with the more efficient compressor, this leaves the smallest amount of compression for the less efficient LRVP to bring the NCG to ambient conditions.

## 4.2 Potential Future Work

In order to increase the accuracy of the thermodynamic model in between the optimum pressure-temperature points selected, it would be beneficial to find more optimum points. This could be done by selecting more condenser outlet temperature points and varying the condenser pressure in order to find which combination of pressure and temperature provides the maximum net power production as was done for Figures 25 through 36 in the appendix. This would decrease the error of the quadratic interpolation of pressure and temperature in Figures 9 and 10.

The accuracy of the model would also be increased by incorporating more data points from the original empirical graph relating the compression ratio, expansion ratio, and air to steam ratio of the SJE. Currently 5 data points from 3 compression ratio curves were used to find a logarithmic relationship between ASR and ER. The 3 logarithmic curves were then quadratically interpolated. Using more data points from the original ASR graph from which Figure 7 was generated would better define each of the compression ratio curves. Also, generating more of these curves would reduce the error introduced by the quadratic interpolation of the selected compression ratio curves. Ultimately this would provide a more accurate motive steam consumption for the SJE analysis and as a result, a more accurate prediction of SJE power consumption.

## APPENDIX

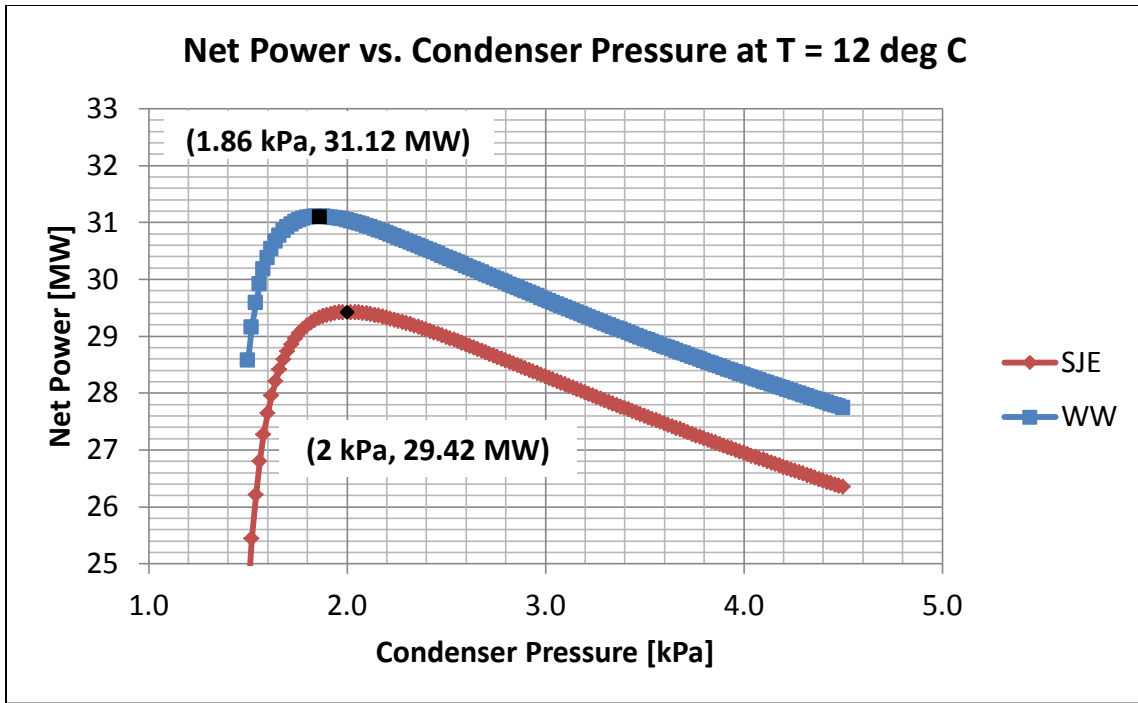


Figure 25: Optimum Pressure at 12° Celsius for Case 1

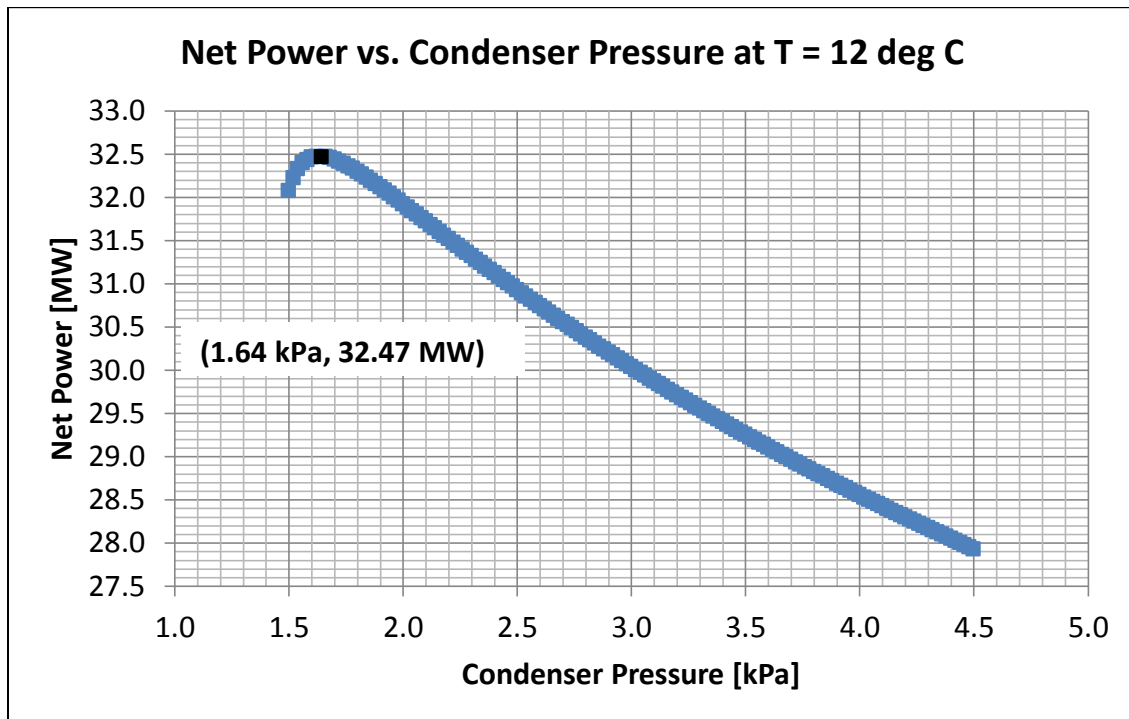


Figure 26: Optimum Pressure at 12° Celsius for Case 2

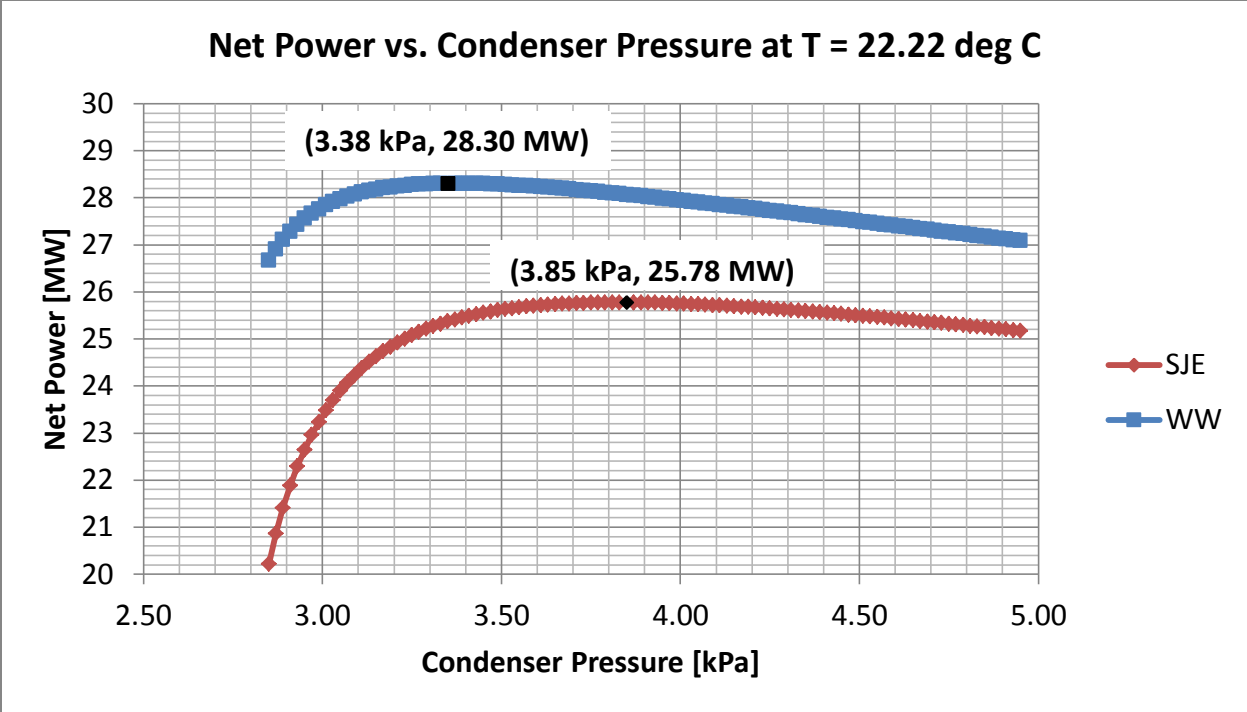


Figure 27: Optimum Pressure at 22.22° Celsius for Case 1

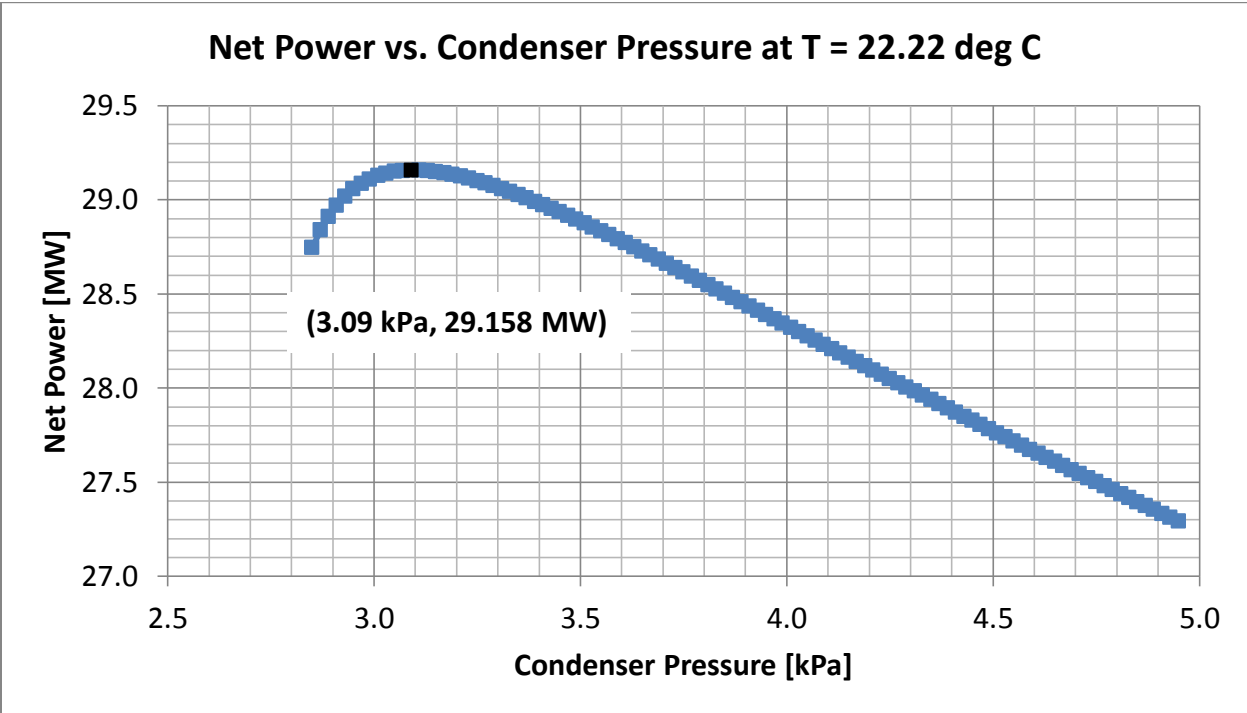


Figure 28: Optimum Pressure at 22.22° Celsius for Case 2

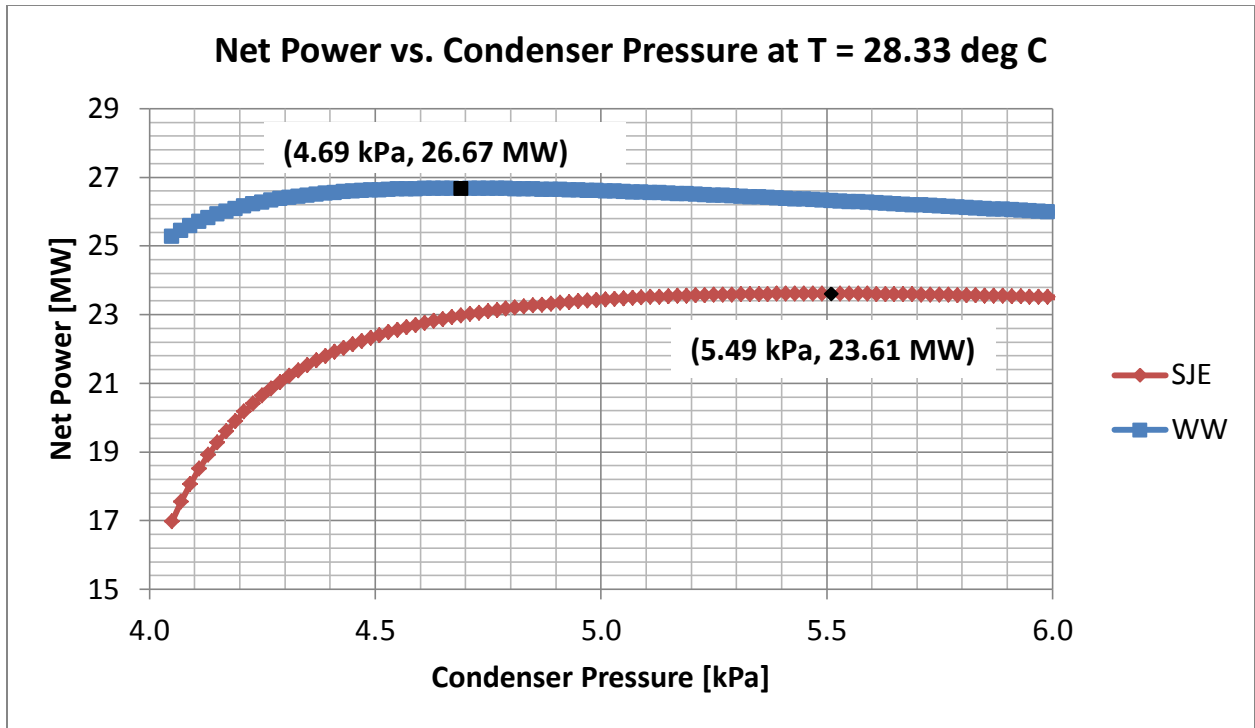


Figure 29: Optimum Pressure at 28.33° Celsius for Case 1

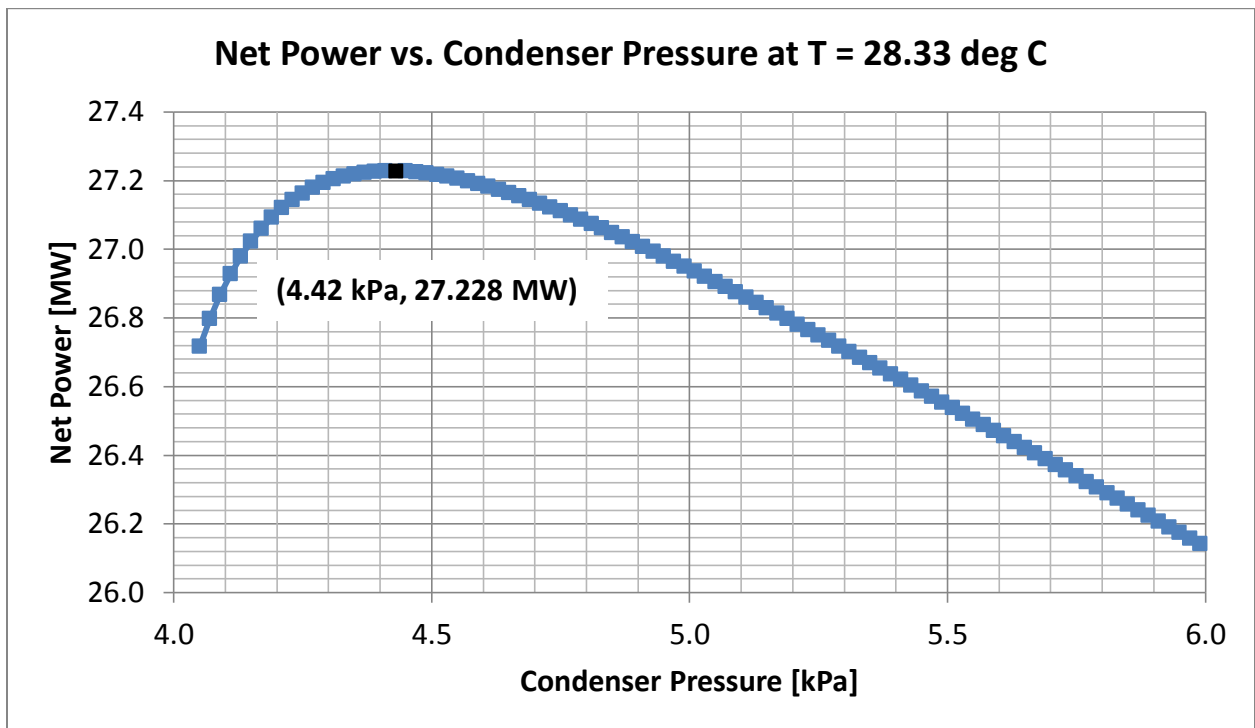


Figure 30: Optimum Pressure at 28.33° Celsius for Case 2

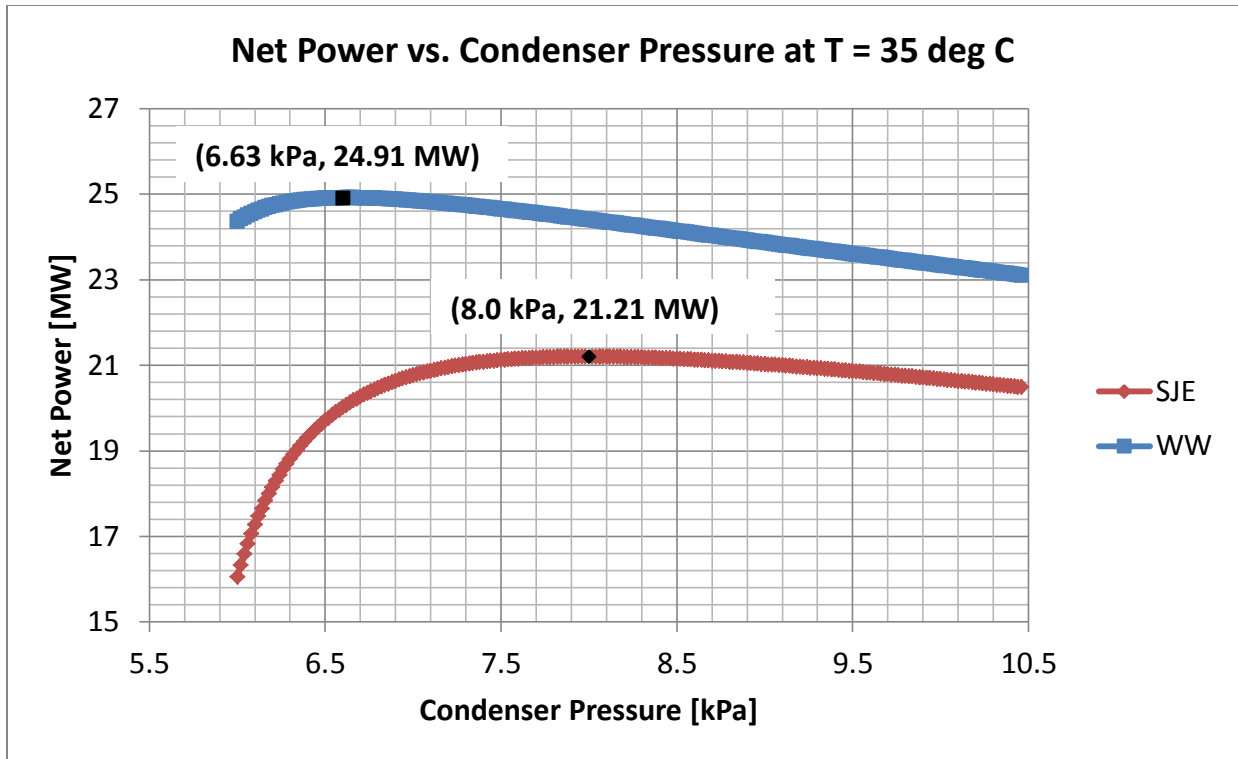


Figure 31: Optimum Pressure at 35° Celsius for Case 1

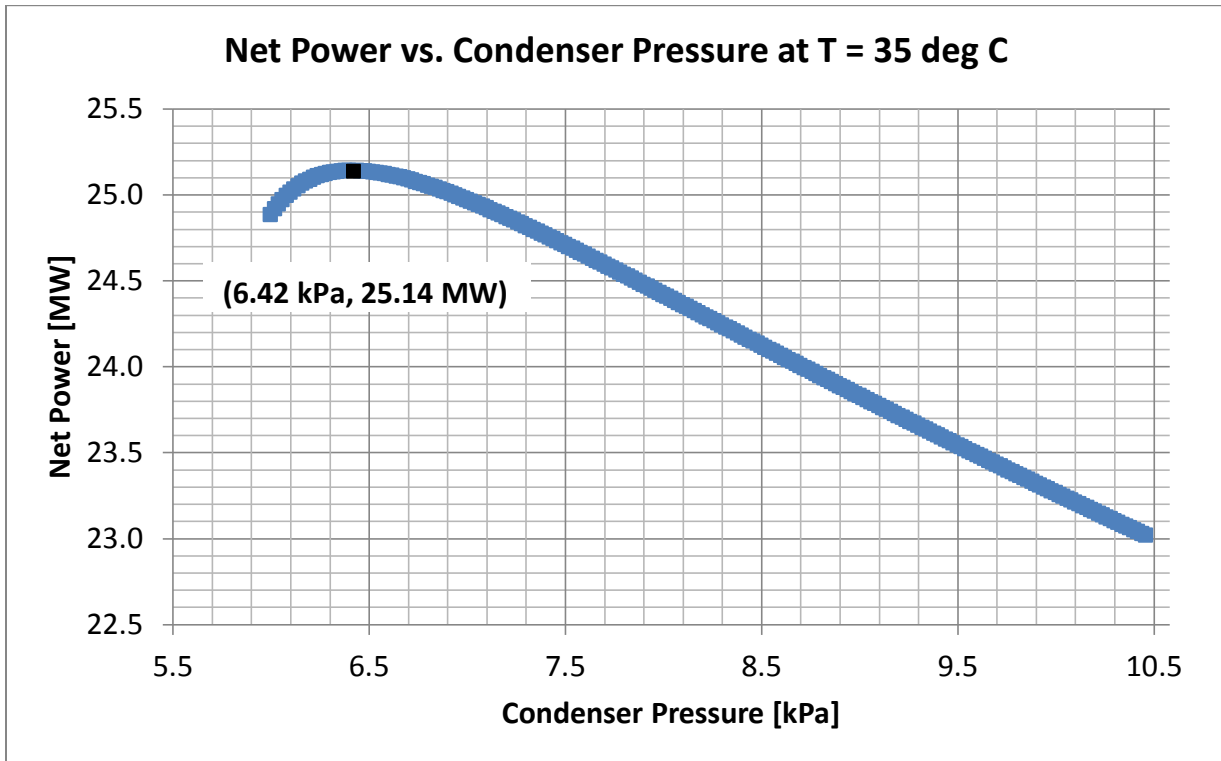


Figure 32: Optimum Pressure at 35° Celsius for Case 2

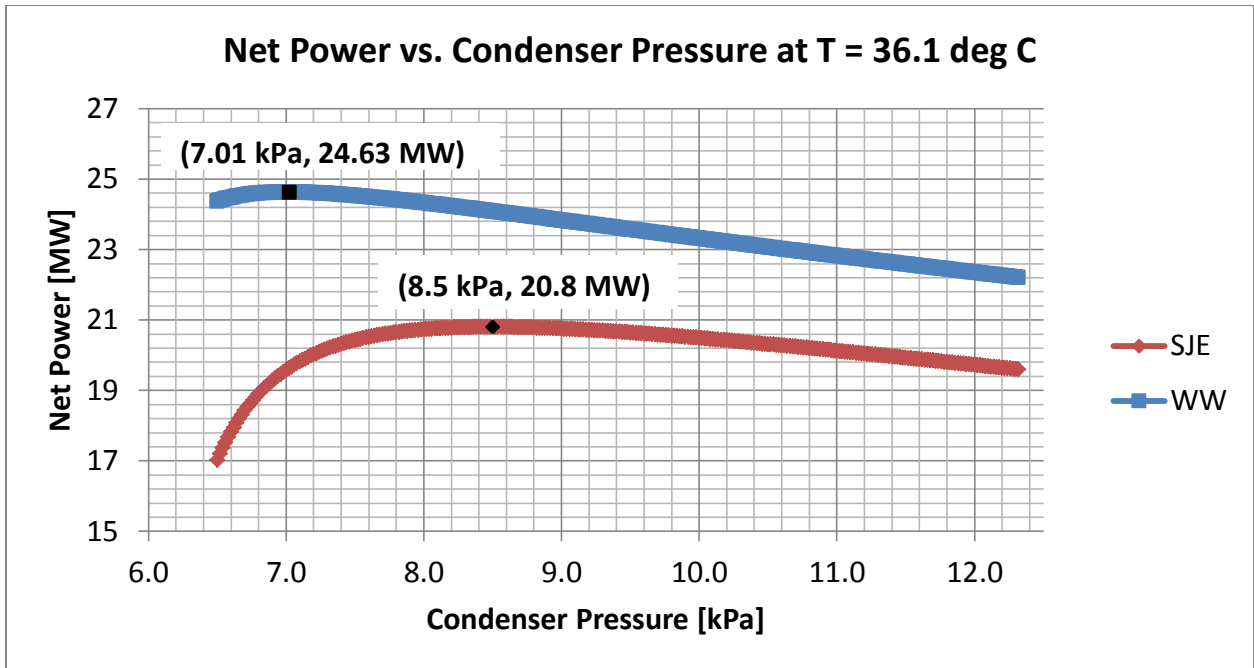


Figure 33: Optimum Pressure at 36.1° Celsius for Case 1

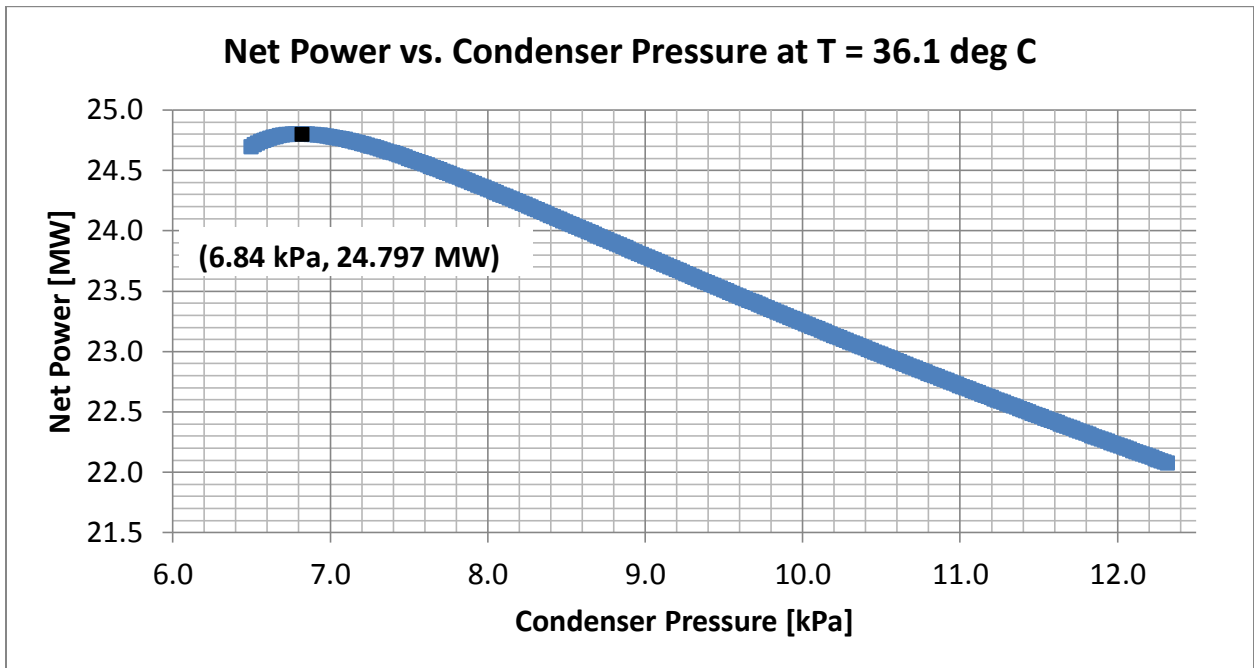


Figure 34: Optimum Pressure at 36.1° Celsius for Case 2

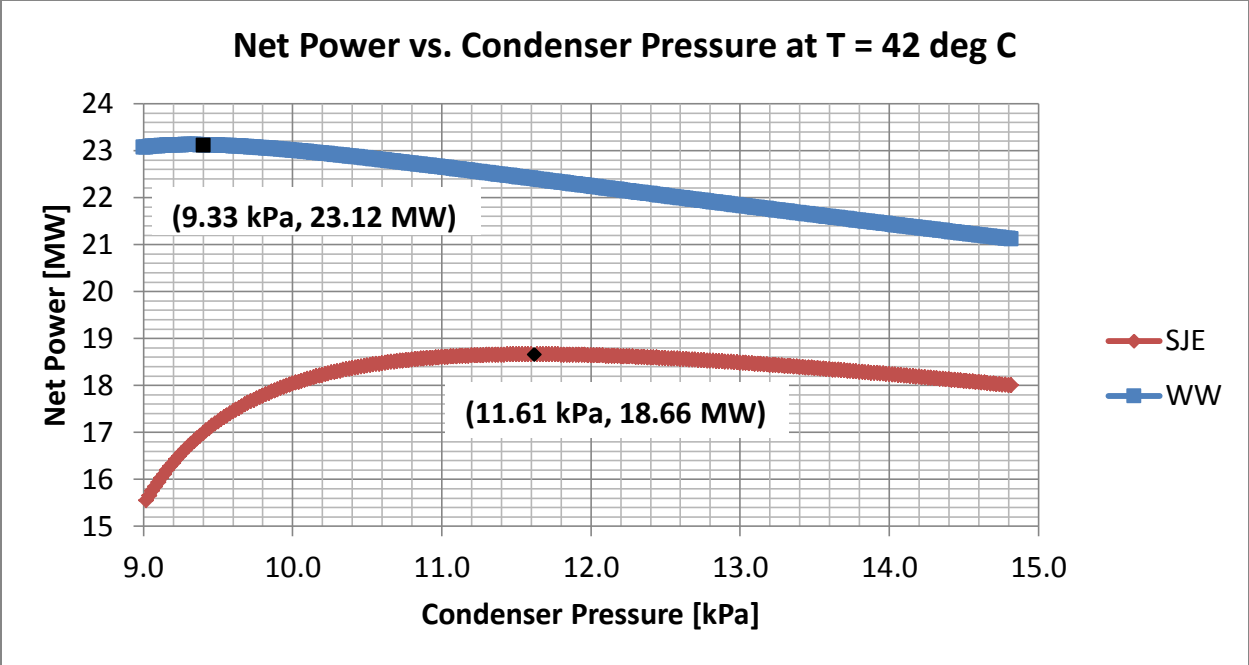


Figure 35: Optimum Pressure at 42° Celsius for Case 1

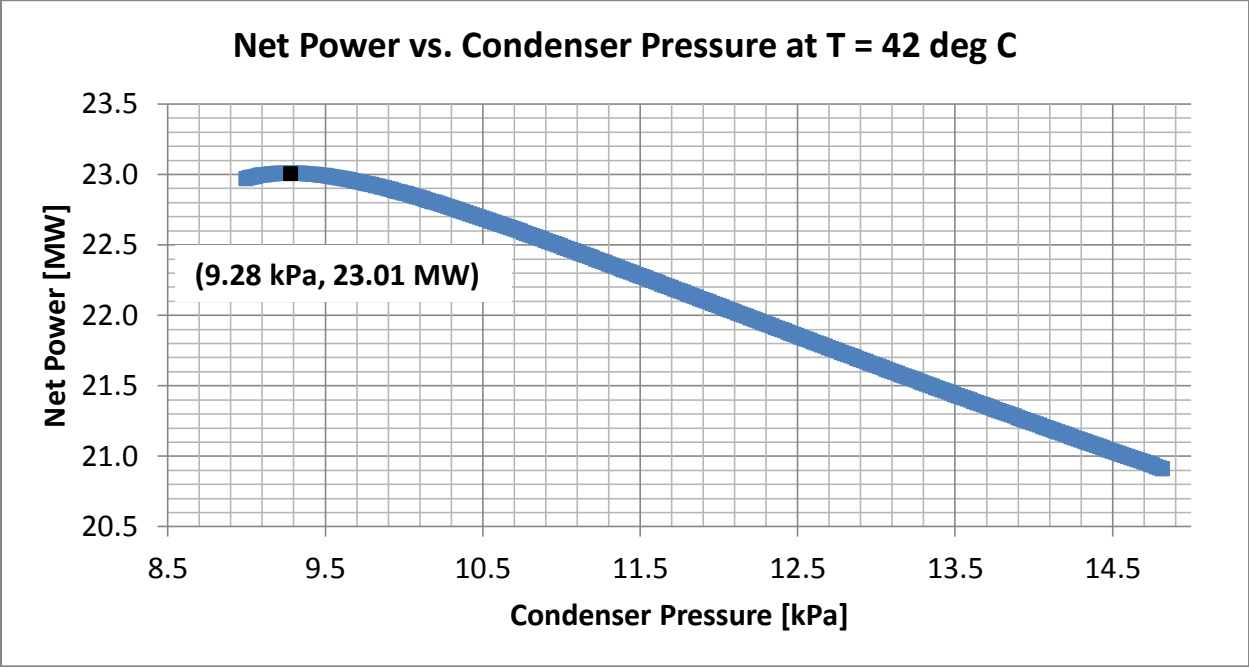


Figure 36: Optimum Pressure at 42° Celsius for Case 2

## REFERENCES

## REFERENCES

1. **Nersesian, Roy L.** *Energy for the 21st Century: A Comprehensive Guide to Conventional and Alternative Sources*. 2nd Edition. M.E. Sharpe, Inc., 2010.
2. *Geothermal Power*. Geothermal. **Enel Green Power**, 2011.  
<<[http://www.enelgreenpower.com/en-GB/plants/renewable\\_energy/geothermal](http://www.enelgreenpower.com/en-GB/plants/renewable_energy/geothermal)>>
3. *Geothermal Basics: Q&A Environmental Benefits*. **Geothermal Energy Association**, Sep. 2012, pp. 9-13, 39.
4. **Khalifa, H. Ezzat and Michaelides Efstathios.** *The Effect of Noncondensable Gases on the Performance of Geothermal Steam Power Systems*. Brown University, Nov. 1978.
5. **Bannwarth, Helmut.** *Liquid Ring Vacuum Pumps, Compressors and Systems*. Liquid Ring Vacuum Pumps and Liquid Ring Compressors. Weinheim: Wiley-VCH, 2005. pp. 192.
6. *Gas Extraction Systems for Geothermal Power Plants*. Costs & Savings. **Nash**, 2010. pp. 9.
7. **El-Dessouky, Hisham et al.** *Evaluation of Steam Jet Ejectors*. Chemical Engineering and Processing. Elsevier, 2002. pp. 552-553.
8. **Santini, Paolo.** *Modular Geothermal Plants in Italy: Technical Characteristics and Operation Results*. Proceedings World Geothermal Conference. General Electric Oil & Gas, 2005.
9. **Forsha, Michael D. et al.** *Development and Operation of a Turbocompressor for Non-condensable Gas Removal at Geothermal Power Plants*. Geothermal Resource Council Transactions, Vol 23, 1999. pp. 59-63.
10. *High-Performance Turbocompressor*. Geothermal Technology. **GRC Bulletin**, 1999. pp. 100
11. **Cappetti, Guido et al.** *Italy Country Update Reprt 1995-1999*. Proceedings World Geothermal Congress. Enel Group. 2000.
12. *Centrifugal Compressors SRL*. GE Oil & Gas. **General Electric**. 2011. pp. 16.
13. **Mueller, Norbert and Janusz Piechna.** *Rotor Apparatus*. US 20,130,336,811 A1United States, December 19, 2013.
14. **Tucker, Robert et al.** *Centrifugal Compressors: Key to Efficient Noncondensable Gas Removal For Geothermal Applications*. Transactions, Vol. 9, Geothermal Resource Council, 1985. pp. 201-205.

15. **Magnus Holmgren and The University of Alabama.** *Thermodynamic Tables Add-in 2.0.8.*
16. **Moran, Michael J. et al.** *Fundamentals of Engineering Thermodynamics.* John Wiley & Sons, Inc., 2011. Table A-21, pp. 926.
17. *Standards for Steam Jet Vacuum Systems.* **Heat Exchange Institute.** 2000. 5th Edition. pp. 29-32.
18. **Millachine, Mauricio Andrés Teke.** *Guidelines for Optimum Gas Extraction System Selection.* University of Iceland, May 2011. pp. 24-26.
19. **Benson, Tom.** *Compressor Thermodynamics.* NASA, 11 July 2008.  
<<<https://www.grc.nasa.gov/www/k-12/airplane/compth.html>>>
20. **Dixon, S. L.** *Fluid Mechanics and Thermodynamics of Turbomachinery.* Elsevier Butterworth-Heinemann. Oxford, 1998. pp. 38.